

COMPARISON OF EMPIRICAL DECLINE CURVE ANALYSIS FOR SHALE
WELLS

A Thesis

by

MOHAMMED SAMI A KANFAR

Submitted to the Office of Graduate Studies of
Texas A&M University
in partial fulfillment of the requirements for the degree of

MASTER OF SCIENCE

Chair of Committee,	Robert A. Wattenbarger
Committee Members,	David S. Schechter
	Yuefeng Sun
Head of Department,	A. Daniel Hill

August 2013

Major Subject: Petroleum Engineering

Copyright 2013 Mohammed Sami A Kanfar

ABSTRACT

This study compares four recently developed decline curve methods and the traditional Arps or Fetkovich approach. The four methods which are empirically formulated for shale and tight gas wells are:

1. Power Law Exponential Decline (PLE).
2. Stretched Exponential Decline (SEPD).
3. Duong Method.
4. Logistic Growth Model (LGM).

Each method has different tuning parameters and equation forms. The main objective of this work is to determine the best method(s) in terms of Estimated Ultimate Recovery (EUR) accuracy, goodness of fit, and ease of matching. In addition, these methods are compared against each other at different production times in order to understand the effect of production time on forecasts. As a part of validation process, all methods are benchmarked against simulation.

This study compares the decline methods to four simulation cases which represent the common shale declines observed in the field. Shale wells, which are completed with horizontal wells and multiple traverse highly-conductive hydraulic fractures, exhibit long transient linear flow. Based on certain models, linear flow is preceded by bilinear flow if natural fractures are present. In addition to this, linear flow is succeeded by Boundary Dominated Flow (BDF) decline when pressure wave reaches

boundary. This means four declines are possible, hence four simulation cases are required for comparison.

To facilitate automatic data fitting, a non-linear regression program was developed using excel VBA. The program optimizes the Least-Square (LS) objective function to find the best fit. The used optimization algorithm is the Levenberg-Marquardt Algorithm (LMA) and it is used because of its robustness and ease of use.

This work shows that all methods forecast different EURs and some fit certain simulation cases better than others. In addition, no method can forecast EUR accurately without reaching BDF. Using this work, engineers can choose the best method to forecast EUR after identifying the simulation case that is most analogous to their field wells. The VBA program and the matching procedure presented here can help engineers automate these methods into their forecasting sheets.

ACKNOWLEDGEMENTS

I would like to express my sincere gratitude to my research advisor and committee chair, Dr. Robert A. Wattenbarger for his valued guidance and inspiration. It has been an honor and a pleasure working with him during the past two years. In addition, I would like to thank Dr. David S. Schechter and Dr. Yuefeng Sun, for serving on my advisory committee. Their constructive feedback helped to greatly improve this work.

I also would like to extend my gratitude to Saudi Aramco for sponsoring me and giving me the opportunity to pursue my advanced degree. Thanks also go to my friends and colleagues and the department faculty and staff for making my time at Texas A&M University a great experience.

Finally, I would like to thank my mother and father for their encouragement and support.

NOMENCLATURE

a	Duong or LGM constant.
A	Area perpendicular to flow, sq-ft
b	Derivative of loss-ratio (Arps' decline exponent), dimensionless
c_t	Total compressibility, psi-1
D	Loss-ratio (Arps' decline constant), Days-1
D_i	Initial loss-ratio, Days ⁻¹
D_1	Loss-ratio at ($t = 1$), Days ⁻¹
D_∞	Loss-ratio at ($t = \infty$), Days ⁻¹
G_p	Cumulative gas production. Mscf
k	Permeability, md
K	Carrying capacity of LGM method.
L_1	Hydraulic fracture spacing, ft
n	Time exponent (hyperbolic exponent).
p	Pressure, psi
q	Flow rate, STB/Day or Mscf/Day
q_1	Flow rate at ($t = 1$), STB/Day or Mscf/Day
q_∞	Flow rate at ($t = \infty$), STB/Day or Mscf/Day
q_i	Flow rate at ($t = 0$), STB/Day or Mscf/Day
q_c	Critical flow rate
Q	Cumulative production, Mscf or STB

Q_{1st}	First calculated cumulative
R^2	Coefficient of determination, fraction
SS_{err}	Error of sum of squares
SS_{res}	Residual of sum of squares
t	Time, Days
t_1	First day of production (usually 1), Days
t_{esr}	Time of end of square-root or time of end of linear flow
t_{last}	Last input time, Days
$t(a, m)$	Duong's time function based on Eqn. 2.12
τ	Characteristic time parameter for SEPD model, Days
T	Temperature, Rankin
v_c	Critical velocity
w_i	Weighting factor at time= i .
\bar{y}	Mean of data
y_i	Data at row i
z	Gas deviation factor, dimensionless

Abbreviations

BDF	Boundary dominated flow
EUR	Estimated ultimate recovery, Bscf or MMSTB
LGM	Logistic growth model
LMA	Levenberg-Marquardt Algorithm
PLE	Power law exponential decline
SEPD	Stretched exponential decline
SRV	Simulated reservoir volume

Greek Symbols

ϕ	Porosity, fraction
μ	Viscosity, cp

TABLE OF CONTENTS

	Page
ABSTRACT	ii
ACKNOWLEDGEMENTS	iv
NOMENCLATURE	v
TABLE OF CONTENTS	viii
LIST OF FIGURES	x
LIST OF TABLES	xiv
CHAPTER I INTRODUCTION	1
1.1 Objective	4
1.2 Thesis Organization	5
CHAPTER II LITERATURE REVIEW	6
2.1 Traditional Decline Curve Methods	7
2.2 Shale Wells Decline Curve Methods	10
2.2.1 Power Law Exponential Decline (PLE)	10
2.2.2 Stretched Exponential Decline (SEPD)	11
2.2.3 Duong’s Method	12
2.2.4 Logistic Growth Model (LGM)	16
CHAPTER III INVESTIGATION OF METHODS	17
3.1 Arps’ Unbounded Reserves Problem and Improvements	17
3.1.1 Composite Arps’ Method	19
3.2 PLE Iteration Blow-up	20
3.3 SEPD Equation Form and Iteration Time Problem	23
3.3.1 The SEPD Method and Long Iteration Convergence Time	24
3.4 Doung’s Method Precautions	26
3.4.1 Duong’s q_{∞} Error and Improvements	26
3.4.2 Error in Linear or Bilinear Flow	26
3.4.3 Material-balance Time Error Results in Recovery Underestimation	27

CHAPTER IV MATCHING AND CALCULATION PROCEDURE	31
4.1 Liquid Loading Filter	31
4.2 Matching Data to Model	32
4.3 EUR Calculations	33
CHAPTER V COMPARISON WITH SIMULATION	35
5.1 Model Description	35
5.2 Simulation and Model Simplifications	37
5.3 Matching Methods to Simulation: A Decline Fit Comparison	41
5.3.1 Case 1 – Linear Flow	41
5.3.2 Case 2 – Linear-BDF	41
5.3.3 Case 3 – Bilinear-Linear Flow	42
5.3.4 Case 4 – Bilinear-Linear-BDF	42
5.4 Effect of Production Time on Forecast	48
5.4.1 Case 1 – Linear Flow	48
5.4.2 Case 2 – Linear-BDF	48
5.4.3 Case 3 – Bilinear-Linear Flow	49
5.4.4 Case 4 – Bilinear-Linear-BDF	49
CHAPTER VI FIELD EXAMPLES	62
6.1 Barnett Shale Gas - Well B-314	62
6.2 Bakken Shale Oil - Well BK-86	64
6.3 Eagleford Shale Gas - Well EF-3	65
6.4 Fayetteville Shale Gas - Well FF-3	66
CHAPTER VII DISCUSSION AND CONCLUSIONS	67
REFERENCES	69
APPENDIX A PLE DERIVATION	71
APPENDIX B DOUNG’S METHOD DERIVATION	73
APPENDIX C TIME AND MATERIAL-BALANCE TIME RELATION	75
APPENDIX D LEVENBERG-MARQUARDT ALGORITHM (LMA)	76

LIST OF FIGURES

	Page
Figure 1. A conceptual vertical well in a conventional oil reservoir was simulated and production is shown by the green curve. Transient flow is relatively short and BDF is reached quickly. Arps exponential decline (marked in red) results in an excellent fit even at an early production time of 3 days.	2
Figure 2. A conceptual horizontal shale-well with multiple traverse hydraulic fractures was simulated and production is shown by the green curve. Arps' method (marked in red) can only fit BDF decline which does not occur until after 700 days of production.	3
Figure 3. Arps' method matches a Fayetteville shale well with a b value greater than 1.	4
Figure 4. Arps' three types of decline and their formulas on a semi-log plot after Arps (1945).	7
Figure 5. Fetkovich Type Curves (1980): A log-log plot with combined radial and BDF declines for various reservoir boundaries. Fetkovich equations for his special dimensionless parameters are also shown.	9
Figure 6. PLE schematic after Ilk et al. (2008). Loss-ratio is modeled uniquely by assuming it follows a power law function at early times and becomes constant at late time.	11
Figure 7. Duong's Type Curves (2011). Curves with different m values are shown. The variable a and m are related by a correlation defined by Duong.	14
Figure 8. A correlation between a and m for various gas plays (Duong 2011).	15
Figure 9. Modified Fetkovich type curve which includes transient linear ($b=2$) and bilinear flow ($b=4$).	18
Figure 10. A simulated shale gas well fitted using the composite Arps method. Arps' equation with $b = 2$ is used until the start of BDF ($tesr$) while $b = 0.16$ is used afterwards.	20
Figure 11. The first matching plot for the PLE method. In this plot, the parameters n , $D1$, and $D\infty$ are found through iteration.	21
Figure 12. The second matching plot of the PLE method. In this plot, iterations find qi	22

Figure 13. The PLE and SEPD methods with the best match found using iteration. Even though both methods are mathematically similar, iteration finds a better match for the PLE method.....	23
Figure 14. A comparison between Excel Solver and LMA. LMA takes less than half the time Excel Solver takes to find the same solution.....	25
Figure 15. A comparison of convergence time between all five methods. The comparison case is infinite acting linear flow lasting for 30 years.....	25
Figure 16. Duong's relationship is actual a relationship between time and material-balance time. Analytical solutions show that m in Duong's equation should be 1. However, substituting $m=1$ in the rate-time relation equation gives an undefined result.	27
Figure 17. Duong's method requires finding the parameter a and m from a plot of time and t_{MB} . The error in t_{MB} leads to obtaining wrong values for m	29
Figure 18. Correction for the first step cumulative eliminates the error in material-balance time.	29
Figure 19. Material-balance time error results in a bad match. Correction for the first step cumulative results in a better match for data. The term q^∞ was constrained to zero for comparison purposes.	30
Figure 20. Illustration of procedure to calculate EUR.	34
Figure 21. Schematic of the Homogenous Model and Naturally Fractured Model. Both models have parallel hydraulic fractures and assume a constant reservoir volume. The naturally fracture models has also parallel naturally fractures that are perpendicular to hydraulic fractures (Tivayanonda et al. 2012).	36
Figure 22. Different ways to visualize fractures in shale wells.	36
Figure 23. Detailed schematics showing the homogenous and naturally fractured model as well as the simulated segments.	38
Figure 24. Case 1: infinite acting linear flow until abandonment.	39
Figure 25. Case 2: linear flow following by boundary dominated flow at around 1000 days.	39
Figure 26. Case 3: Bilinear flow followed by linear flow which lasts until abandonment.	40

Figure 27. Case 4: The case has all three flow regimes. Bilinear then linear then BDF.....	40
Figure 28. The final iteration match for the Arps Method. Arps Fit Case 1 Perfectly. Arps' method does not fit the other cases accurately because it cannot model multiple flow regimes.	43
Figure 29. The final iteration match for the PLE method. The PLE method fits Case 1 perfectly and fairly fits Case 2 and 4. Case 3, however, is fitted by coincidence here and might not fit other scenarios similar to case 3 as accurately.	44
Figure 30. The final iteration match for the SEPD method. The sped method fits gives a good coefficient of determination in most cases however it does not capture the shape. Case 2 is the only case where the method captures the shape.	45
Figure 31. The final iteration match for the Duong method. Does method fairly captures the shape of Case 1 and 3. The other cases are poorly matched.	46
Figure 32. The final iteration match for the LGM method. The method goods good fit and curve shapes however it does not capture the shape of BDF.	47
Figure 33. Case 1 forecast comparison with 100 days of production data.....	50
Figure 34. Case 1 forecast comparison with 1000 days of production data.....	51
Figure 35. Case 1 forecast comparison with 9000 days for production data.	52
Figure 36. Case 2 forecasts comparison with 1000 days of production data. All methods forecast the wrong production because during transient flow the time of BDF decline cannot be determined with production data alone.	53
Figure 37. Case 2 forecast comparison with 3000 days of production data. The PLE method is the only method that captures the decline and forecast a correct recovery.	54
Figure 38. Case 2 forecast comparison with 9000 days of production data.....	55
Figure 39. Case 3 forecast comparison with 100 days of production data. None of the methods can forecast the correct production at such early production time.	56

Figure 40. Case 3 forecast comparison with 1000 days of production data. The Arps method overestimates recovery while the LGM Method underestimates. The other three methods forecast production accurately.	57
Figure 41. Case 3 forecast comparison with 9000 days of production data. All methods converge at the true match except Arps which is slightly overestimating.	58
Figure 42. Case 4 forecast comparison with 1000 days of production data. None of the methods forecast the true production because the time of BDF decline cannot be determined with production data alone.	59
Figure 43. Case 4 forecast comparison with 3000 days of production. The PLE and LGM methods capture the true profile.	60
Figure 44. Case 4 forecast comparison with 9000 days of production. The PLE and LGM are still the best. The other methods slightly overestimate recovery.	61
Figure 45. Barnett Well B-314. The well exhibits linear flow and BDF. The best method when BDF is reached is the PLE method. The other methods should converge as production time increase.	63
Figure 46. Linear flow for Bakken shale oil well BK-86. This well is similar to Case 1 or 2. For Case 1, Arps, LGM and PLE methods provide comparable forecasts assuming linear flow regime until abandonment. For Case 2 the forecast has to be re-run when BDF is reached.	64
Figure 47. Eagleford well 204. This well is similar to case 3 or 4. For Case 3 the true forecast should be bracketed between Arps and the LGM method. For Case 4 the forecast has to be re-run when BDF is reached.	65
Figure 48. Fayetteville Well FF-3. The well is not similar to any of the run cases. The best method cannot be determined.	66

LIST OF TABLES

	Page
Table 1 – Arps equations for rate and cumulative (1945).....	8

CHAPTER I

INTRODUCTION

Historically, the decline curve analysis method by Arps (1945) has been the most popular tool for forecasting Estimated Ultimate Recovery (EUR) and reserves because of its reliability and simplicity. In recent years, the industry started producing shale plays and production forecast analysis for shale wells is problematic using this traditional method. The reason is that Arps' equations only work during Boundary Dominated Flow (BDF) decline. Unlike in conventional reservoirs, such decline is not observed in shale wells during early production life when financial forecast is important (Figure 1-Figure 2). Arps' method match shale wells with b values greater than what Arps specified (Figure 3). To eliminate this problem and improve shale production forecast, researchers developed new empirical methods. However, the new methods have different equation forms and often result in dissimilar forecasts.

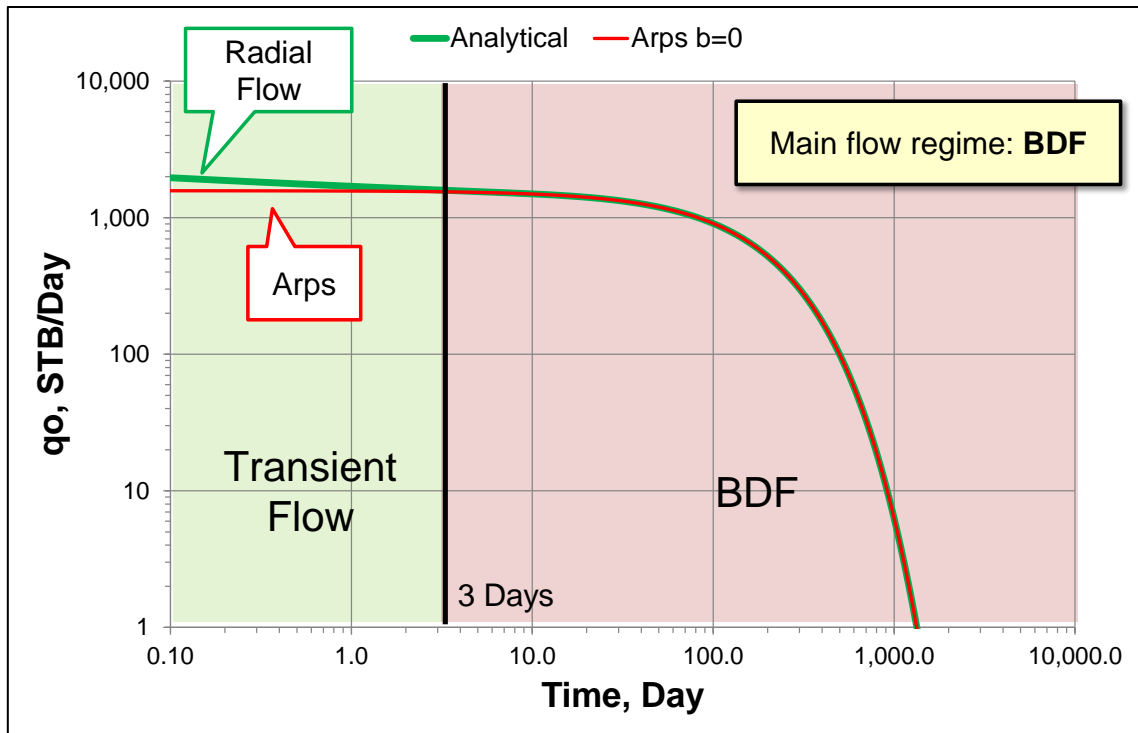


Figure 1. A conceptual vertical well in a conventional oil reservoir was simulated and production is shown by the green curve. Transient flow is relatively short and BDF is reached quickly. Arps exponential decline (marked in red) results in an excellent fit even at an early production time of 3 days.

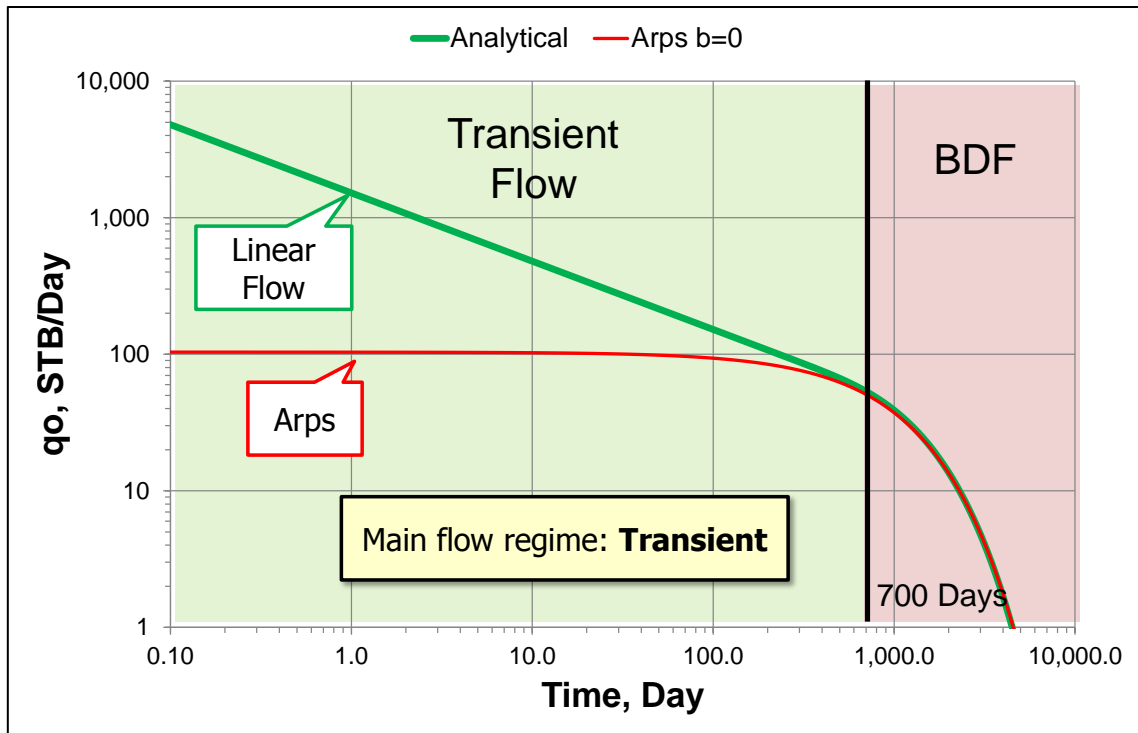


Figure 2. A conceptual horizontal shale-well with multiple traverse hydraulic fractures was simulated and production is shown by the green curve. Arps' method (marked in red) can only fit BDF decline which does not occur until after 700 days of production.

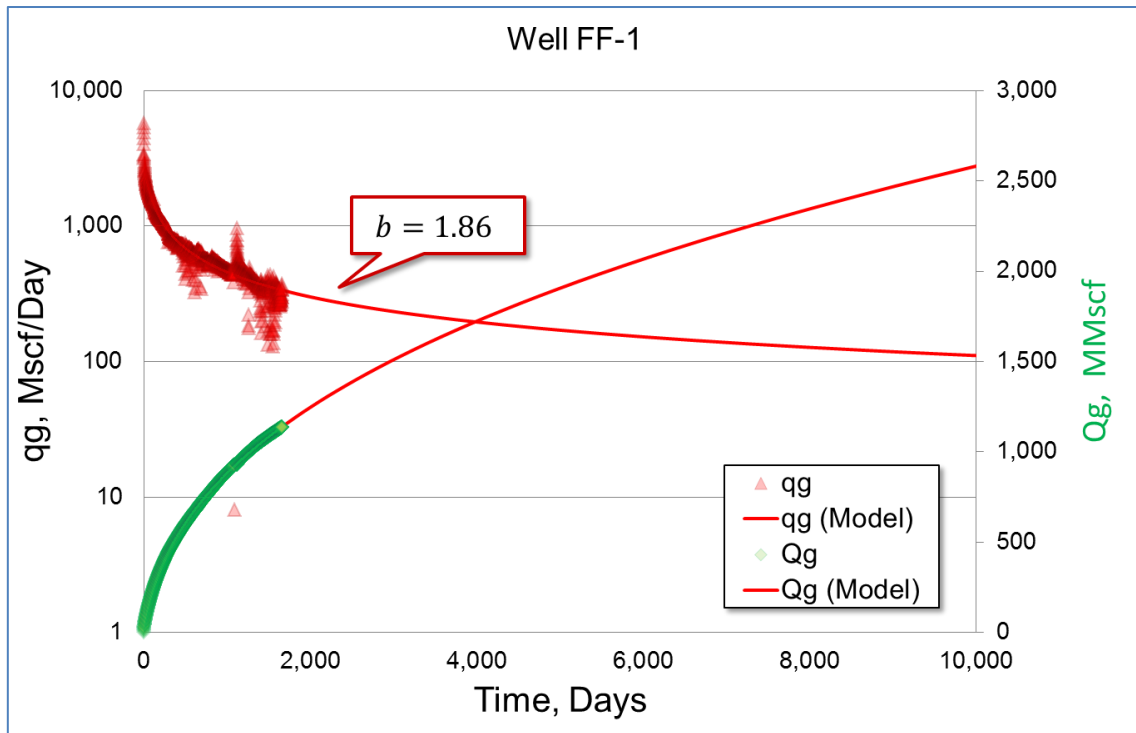


Figure 3. Arps' method matches a Fayetteville shale well with a b value greater than 1.

1.1 Objective

The main purpose of this work is to identify the most accurate method(s) by comparing it/them to analytical and conceptual simulation models. Analytical and simulation models are used for benchmarking because they are applied, validated, and well established in literature (Ahmadi et al. 2010; Bello and Wattenbarger 2008; Bello and Wattenbarger 2010; Samandarli et al. 2011). Other objectives of this work include identifying of strengths and weaknesses of each empirical method and establishing a workflow to automatically match methods to data using non-linear regression. The methods are compared in terms of:

1. Ultimate recovery accuracy
2. Goodness of fit
3. Ease of matching

1.2 Thesis Organization

This thesis is divided into seven chapters. The organization of these chapters is as follows:

Chapter I is an introduction to the subject of this research, its motivations and objectives.

Chapter II is a literature review including history of empirical decline curve analysis and the traditional decline curve methods of Arps and Fetkovich. The chapter also reviews recent empirical decline methods that are developed specifically for tight gas and shale wells.

Chapter III investigates the advantages and shortcomings of the new methods. It also shows problems that engineers might encounter while applying the methods as well as procedures to mitigate such problems.

Chapter IV describes the proposed procedure for matching and forecasting.

Chapter V compares the new decline methods and the traditional methods against conceptual simulation models. The methods which best fit simulation cases and predict their EUR are determined.

Chapter VI shows field examples and applications of the proposed methodology.

Chapter VII presents discussion and conclusions.

CHAPTER II
LITERATURE REVIEW

The fundamental idea of decline curve analysis is to forecast production based on rates from previous production. The first reference to such method is by Arnold and Anderson (1908). Later, Johnson and Bollen (1927) introduces the concept of loss-ratio which represents the slope of rate versus time on a semi-log plot and Pirson (1935) concludes that some wells have constant loss-ratio while others have constant derivative of loss-ratio.

The loss-ratio is defined as,

$$\frac{1}{D} = -\frac{q}{dq/dt} \dots\dots\dots (2.1)$$

Loss-ratio derivative is defined as,

$$b = \frac{d}{dt} \left[-\frac{q}{dq/dt} \right] \dots\dots\dots (2.2)$$

2.1 Traditional Decline Curve Methods

Arps' decline curve analysis is based on graphically extrapolating production on a semi-log plot ($\log q$ vs. t) to abandonment. Arps identifies three types of production rate decline during BDF: Exponential, Hyperbolic or Harmonic. Arps introduces equations for each type and used the concept of loss-ratio and its derivative to derive the equations. The three declines have b values ranging from 0 to 1. Where $b = 0$ represents the exponential decline, $0 < b < 1$ represents the hyperbolic decline, and $b = 1$ represents the harmonic decline (Figure 4). Equations for forecasting cumulative production or EUR is shown in Table 1.

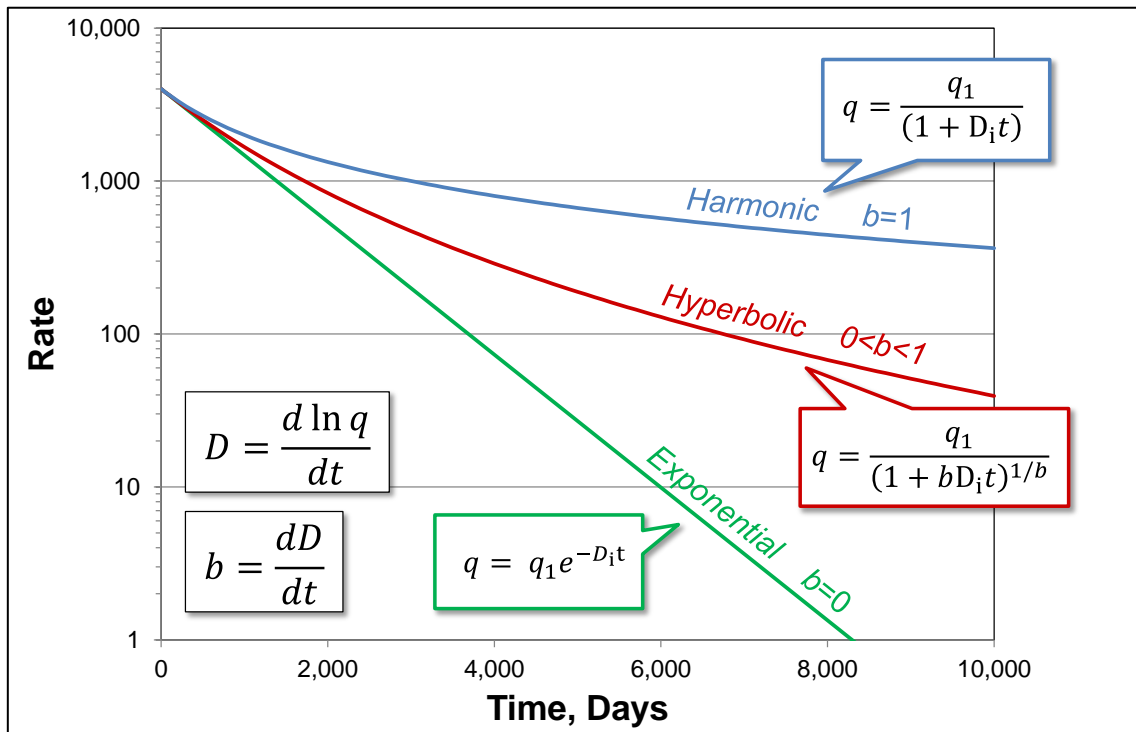


Figure 4. Arps' three types of decline and their formulas on a semi-log plot after Arps (1945).

Fetkovich (1980) supports Arps' exponential decline formula with physical theory. In his work, Fetkovich combines transient radial flow solutions with Arps' BDF decline formulas to form log-log type curves. Because the end of radial flow and start of BDF can vary based on distance to boundary, Fetkovich uses special dimensionless rate and time plotting functions to collapse all solutions at a single end of radial flow time. Fetkovich type curves and his special dimensionless plotting functions are shown in Figure 5.

Table 1 – Arps equations for rate and cumulative (1945).

Exponential ($b = 0$)	Hyperbolic ($0 < b < 1$)	Harmonic ($b = 1$)
D = constant	D = changing	D = changing
$q = q_0 e^{-tD_i}$	$q = q_0 (1 + bD_i t)^{-\frac{1}{b}}$	$q = q_0 (1 + bD_i t)^{-\frac{1}{b}}$
$Q = \frac{(q_0 - q)}{D_i}$	$Q = \frac{q_0^b}{D_i(1-b)} (q_0^{1-b} - q^{1-b})$	$Q = \frac{q_0}{D_i} (\log q_0 - \log q)$

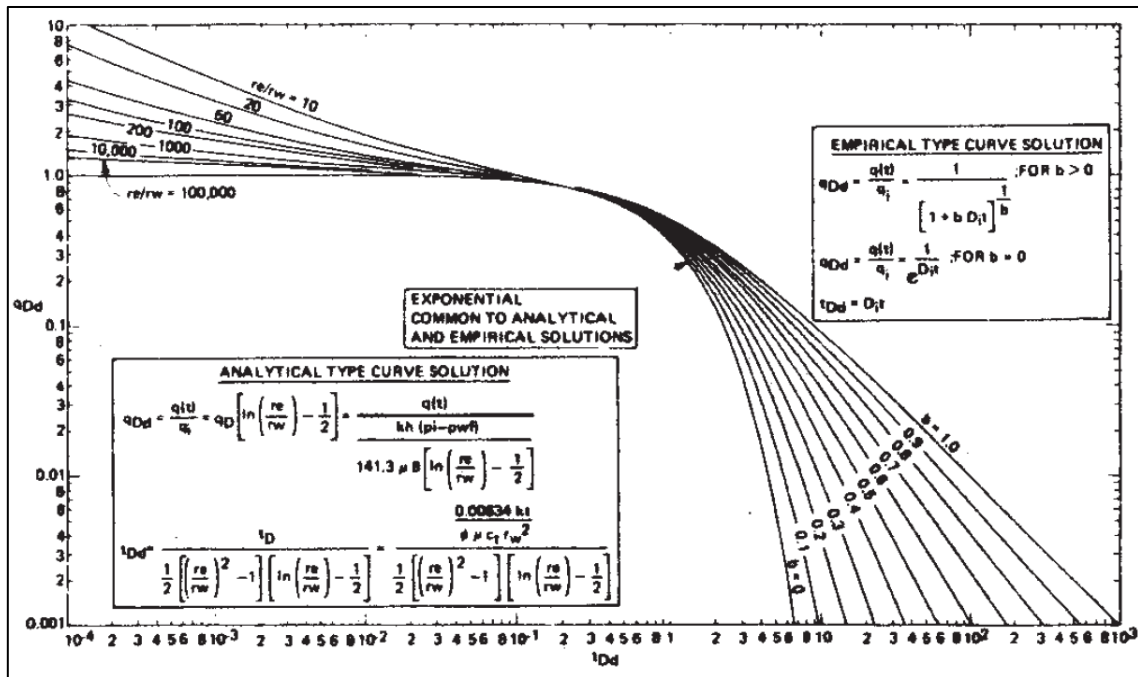


Figure 5. Fetkovich Type Curves (1980): A log-log plot with combined radial and BDF declines for various reservoir boundaries. Fetkovich equations for his special dimensionless parameters are also shown.

The Arps or Fetkovich approach usually limits the value of b to $(0 \leq b \leq 1)$. However, for shale wells it is often observed that values of $b > 1$ seem to match field data. Lee and Sidle (2010) showed that $b > 1$ gives physically impossible results when Arps' cumulative production equation is evaluated at infinite time. Therefore, new methods to overcome these challenges are developed.

2.2 Shale Wells Decline Curve Methods

2.2.1 Power Law Exponential Decline (PLE)

Ilk et al. (2008) introduces the Power Law Exponential (PLE) decline method to better fit and forecast tight gas and shale production. The PLE models the loss-ratio uniquely by assuming that the loss-ratio follows a power law function at early time and becomes constant at late time (Figure 6). This formulation of loss-ratio can be substituted into the original definition of the loss-ratio and integrated to give the PLE rate-time relation. The derivation of the PLE is demonstrated in Appendix A.

PLE loss-ratio,

$$D = D_{\infty} + D_1 t^{-(1-n)} \dots\dots\dots (2.3)$$

PLE derivative of loss-ratio,

$$b = \frac{-D_1(n-1)t^n}{(D_{\infty}t + D_1t^n)^2} \dots\dots\dots (2.4)$$

PLE rate-time relation,

$$q = q_i \exp\left(-D_{\infty}t - \frac{D_1}{n}t^n\right) \dots\dots\dots (2.5)$$

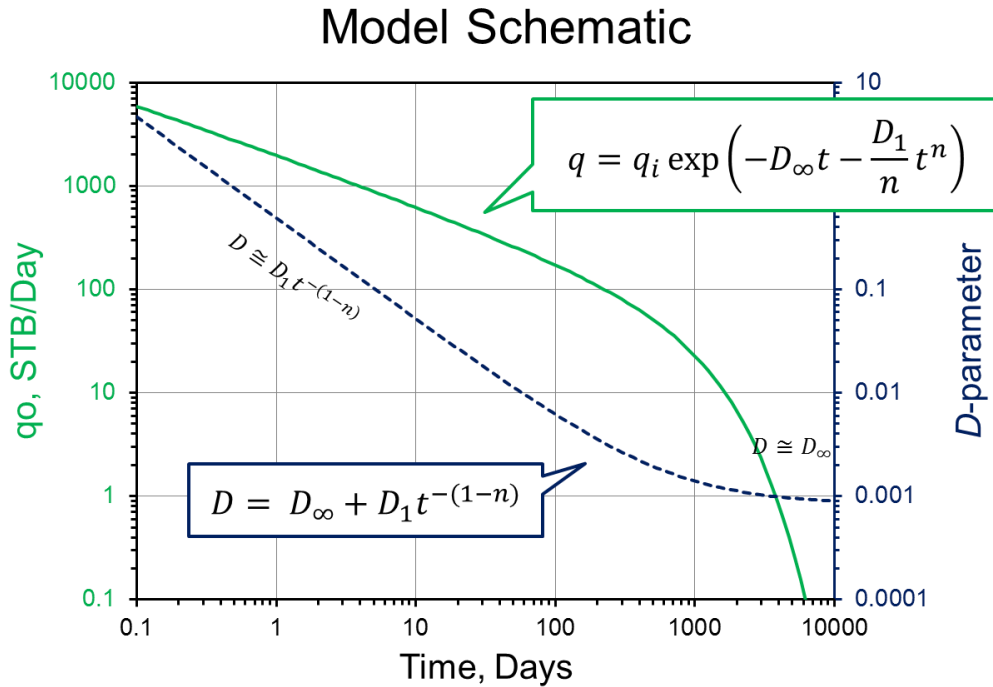


Figure 6. PLE schematic after Ilk et al. (2008). Loss-ratio is modeled uniquely by assuming it follows a power law function at early times and becomes constant at late time.

2.2.2 Stretched Exponential Decline (SEPD)

Valko (2009) independently proposes the Stretched Exponential Decline (SEPD) which is similar to the PLE method. Valko uses this method to evaluate the effect of stimulation (re-stimulation) treatment in Barnett shale by analyzing monthly production from public databases. Later, Valko and Lee (2010) use this method for forecasting.

SEPD rate-time relation,

$$q = q_i \exp \left[- \left(\frac{t}{\tau} \right)^n \right] \dots\dots\dots (2.6)$$

SEPD cumulative-time relation,

$$Q = \frac{q_i \tau}{n} \left\{ \Gamma \left[\frac{1}{n} \right] - \Gamma \left[\frac{1}{n}, \left(\frac{t}{\tau} \right)^n \right] \right\} \dots\dots\dots (2.7)$$

The SEPD equation differs from the PLE model in not considering the behavior at late times (the D_∞ term). In the SEPD method, D_∞ is always considered to be zero and τ is equivalent to $(n/D_1)^{1/n}$. One advantage of SEPD over PLE is the provided cumulative-time relation. This relation adds the option of fitting data to cumulative production, which is smoother and easier to regress on than the usually scattered production rate trends. In the cumulative equation, the first term inside the brackets is the complete gamma function and the second term is the incomplete gamma function.

2.2.3 Duong's Method

Duong's method (2011) is developed on the basis that production rate and time have a power law relation or form a straight line when plotted on a log-log scale. Integrating this relation with respect to time from (0 to t) gives a relationship between time and material balance time (equation 3.8).

Duong's time/material-balance-time relation,

$$\frac{q}{G_p} = at^{-1} \dots\dots\dots (2.8)$$

Using this relation, the variable a is 1/2 for linear flow and 3/4 for bilinear flow. Duong made the above equation more flexible to match field data by substituting m for the time exponent. Differentiating this equation with respect to time and integrating (from 1 to t) give Duong's rate-time relation. Duong's equations are shown below.

Duong's modified time/material-balance-time relation,

$$\frac{q}{G_p} = at^{-m} \dots\dots\dots (2.9)$$

Duong's rate-time relation,

$$q = q_1 t(a, m) + q_\infty \dots\dots\dots (2.10)$$

Duong's cumulative-time relation,

$$G_p = \frac{q_1 t(a, m)}{at^{-m}} \dots\dots\dots (2.11)$$

where,

$$t(a, m) = t^{-m} \exp\left(\frac{a}{1-m} (t^{1-m} - 1)\right) \dots\dots\dots (2.12)$$

Duong adapts the concept of expanding Stimulated Reservoir Volume (SRV) which means that production never reaches BDF. This concept is based on reactivating existing faults and fractures caused by local stress changes during depletion (Warpinski and Branagan 1989). Nonetheless, Duong adds the term q_∞ to the rate-time equation to better fit field data. Duong's method is the only method that models fracture fluid clean-up as shown by Duong's type curves (Figure 7). In Duong's type curves, the variable a and m are correlated by analyzing various gas plays (Figure 8).

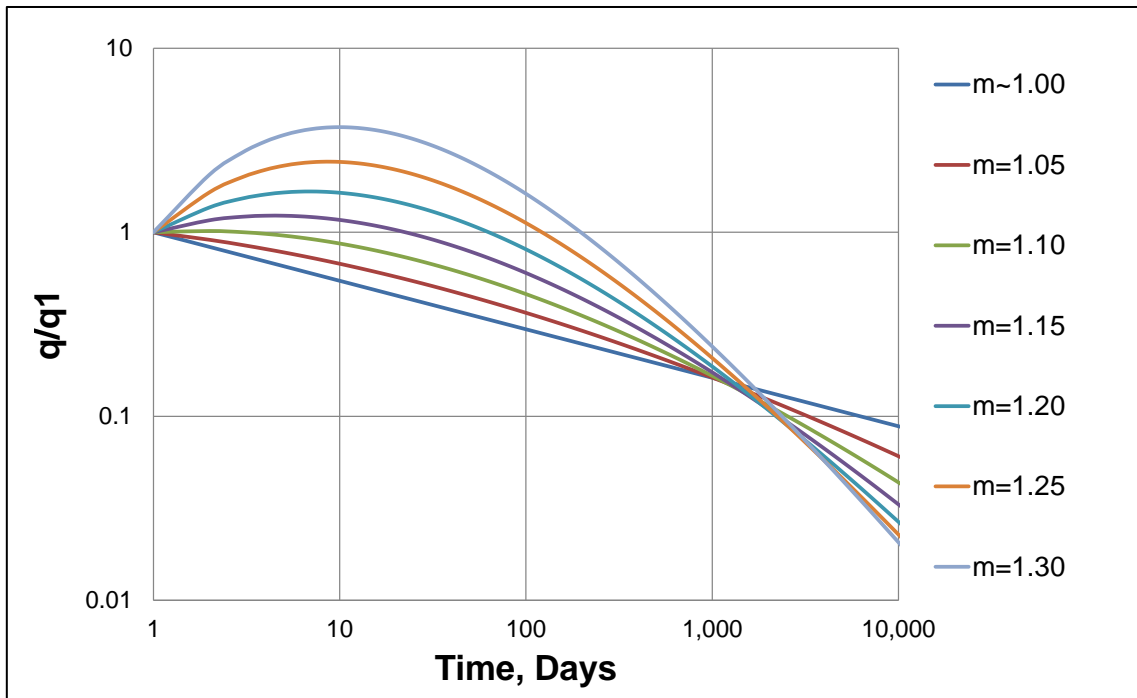


Figure 7. Duong's Type Curves (2011). Curves with different m values are shown. The variable a and m are related by a correlation defined by Duong.

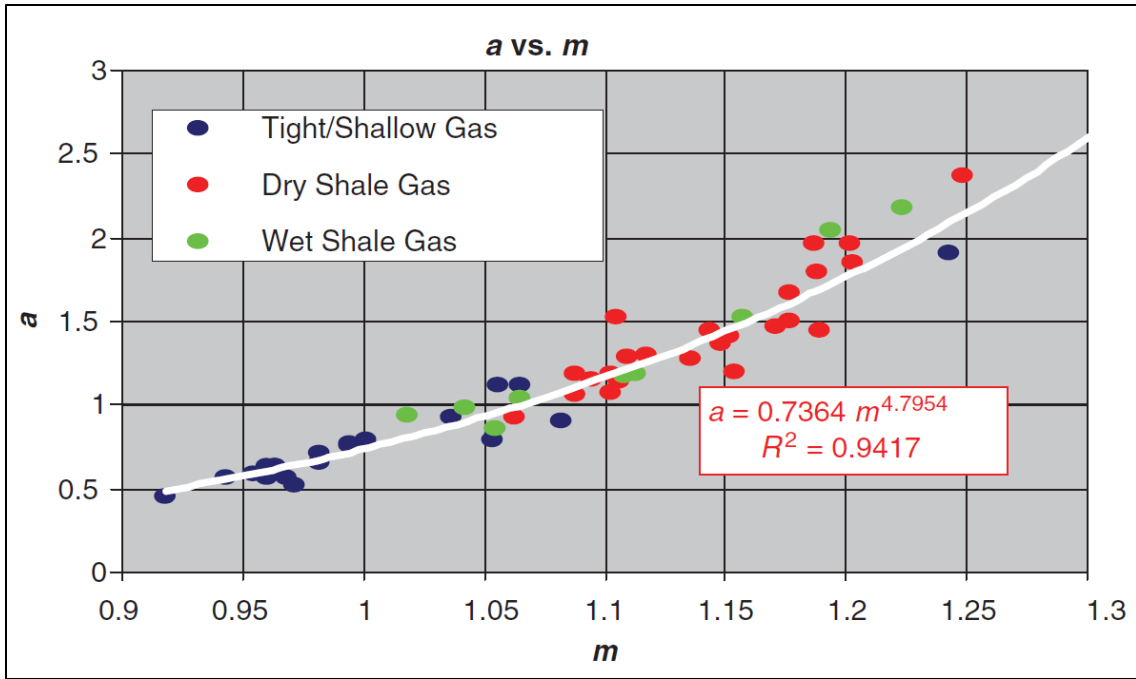


Figure 8. A correlation between a and m for various gas plays (Duong 2011).

2.2.4 Logistic Growth Model (LGM)

Logistic Growth Models (LGM) are based on the concept that growth is possible only to a certain size. The maximum growth size possible is referred to as the carrying capacity (K). LGMs are used to model population growth and its first adaptation in the petroleum industry is by Hubbert's (1956). The Hubbert's model is used to model production of a field or region. Clark et al. (2011) develops a similar model but to forecast production from a single well. The model is adapted from another LGM that models liver regrowth hyperbolically. The rate and cumulative equations are the defined below.

LGM rate-time relation,

$$q = \frac{Knat^{n-1}}{(a + t^n)^2} \dots\dots\dots (2.13)$$

LGM cumulative-time relation,

$$Q = \frac{Kt^n}{a + t^n} \dots\dots\dots (2.14)$$

CHAPTER III

INVESTIGATION OF METHODS

The previous chapter provided an overview of both traditional and new empirical decline methods. This chapter shows the drawback and advantages of each method and provides simple solutions to mitigate difficulties which might be encountered while applying the methods.

3.1 Arps' Unbounded Reserves Problem and Improvements

Arps' equations are designed for BDF decline and the reason shale wells have b values greater than 1 is the fact that shale wells are generally in transient flow. Shale has low permeability and is usually produced from hydraulically fracture wells. This results in a long transient linear or bilinear flow which can be fitted using Arps' hyperbolic equation and b values of 2 or 4 respectively (Figure 9). However, these values are outside the range that Arps' specified ($0 \leq b \leq 1$) and result in two problems. The first problem is that extrapolation on transient flow overestimates reserves. The second problem is that the hyperbolic equation with b values greater than one never goes to zero and therefore reserves is unbounded. Lee and Sidle (2010) demonstrated the second problem with the following:

Arps' hyperbolic cumulative equation,

$$Q = \frac{q_i^b}{D_i(1-b)} (q_i^{1-b} - q^{1-b}) \dots\dots\dots (3.1)$$

At infinite time, rate should be zero and therefore, substituting a rate of zero and b value greater than 1 give undefined results,

$$\lim_{t \rightarrow \infty} Q = \frac{q_i^2}{-D_i} \left(\frac{1}{q_i} - \frac{1}{q_\infty} \right) = \text{Undefined} \dots\dots\dots (3.2)$$

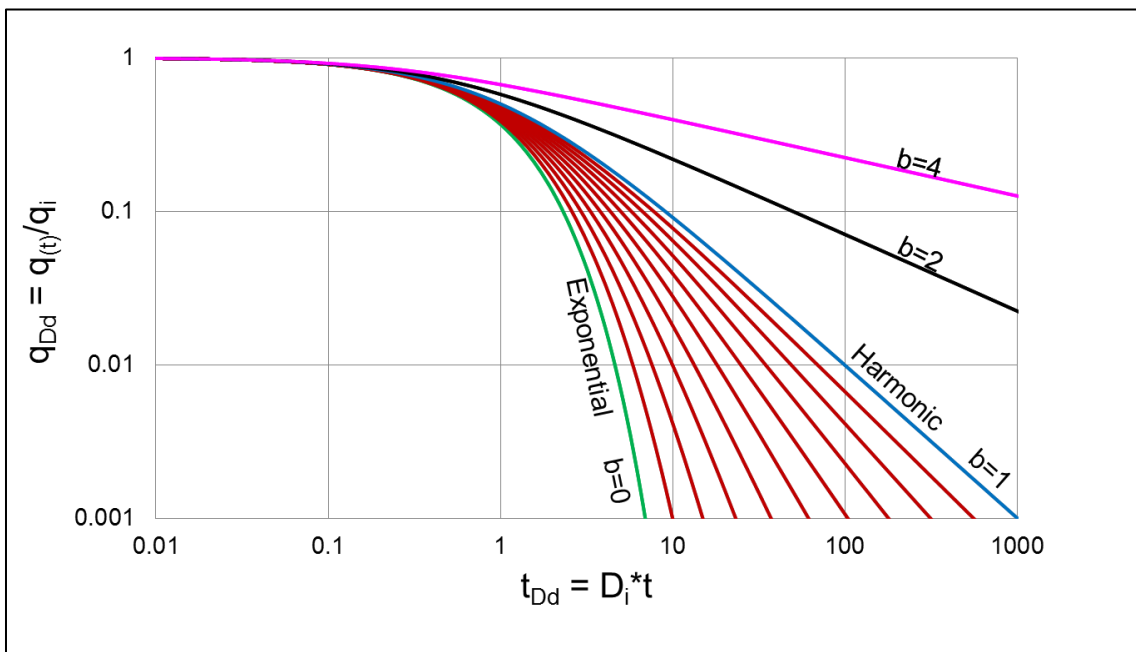


Figure 9. Modified Fetkovich type curve which includes transient linear ($b=2$) and bilinear flow ($b=4$).

3.1.1 Composite Arps' Method

This study proposes a methodology to mitigate both aforementioned problems by using a composite Arps' forecast. We recommend using Arps' hyperbolic equation with b values of 2 for linear flow or 4 for bilinear flow until start of BDF decline. Afterwards, a b value of 1 or less should be used to match the BDF decline. If start of BDF is not known, it can be calculated using equation 3.3. The methodology is illustrated in Figure 10. In some cases when rates and pressure are variable, a perfect match with ($b=2$ or $b=4$) is no possible unless rate is normalized with pressure.

Time to start of BDF decline,

$$t_{esr} = \frac{0.25}{0.00633} (\phi\mu c_t)_i \frac{L_1^2}{4k} \dots\dots\dots (3.3)$$

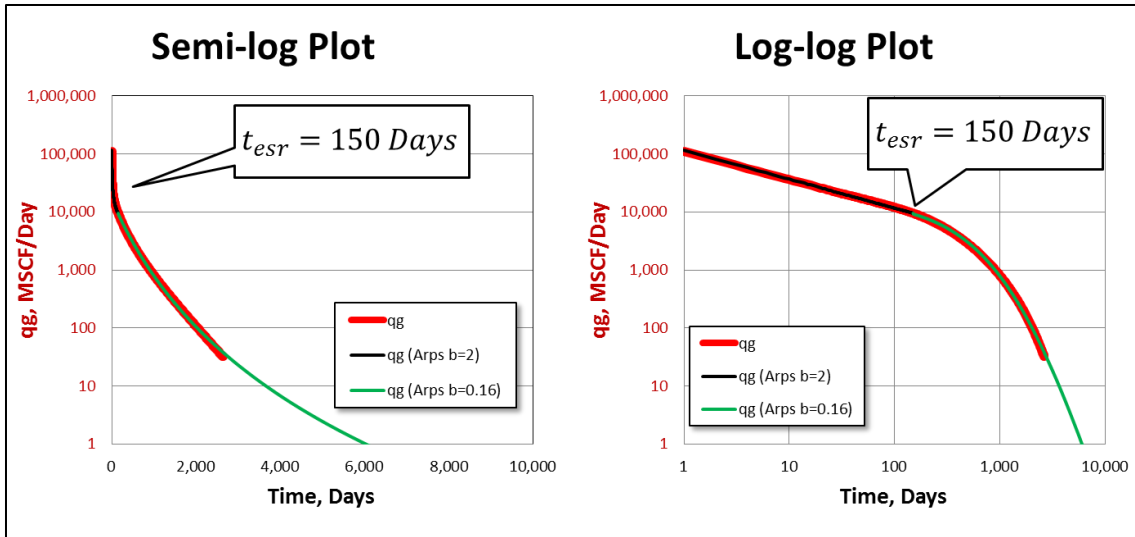


Figure 10. A simulated shale gas well fitted using the composite Arps method. Arps' equation with $b = 2$ is used until the start of BDF (t_{esr}) while $b = 0.16$ is used afterwards.

3.2 PLE Iteration Blow-up

The PLE method requires fitting on two different plots. The first plot is a log-log plot of loss-ratio versus time (Figure 11). The parameters n , D_1 , and D_∞ are obtained from this plot. The parameter n is the slope, the parameter D_1 is the intercept, and the parameter D_∞ is the value of loss-ratio at infinite time. The second plot is either a semi-log or log-log plot of rate versus time and it is used to find the parameter q_i (Figure 12). We fitted various cases using the PLE model using non-linear regression. In many cases, the best match for q_i is very large and exceeds the range that excel can handle. The reason q_i is very large is that parameter n is small. This can be illustrated by rearranging the rate-time relation (equation 2.5) to equation 3.4. If parameter n is small, the solution q_i becomes too large because of the exponential function. The range for positive values

for a double variable in Microsoft Excel is from 4.94065645841247E-324 to 1.79769313486232E308.

$$q_i = \frac{q}{\exp\left(-D_\infty t - \frac{D_1}{n} t^n\right)} \dots\dots\dots (3.4)$$

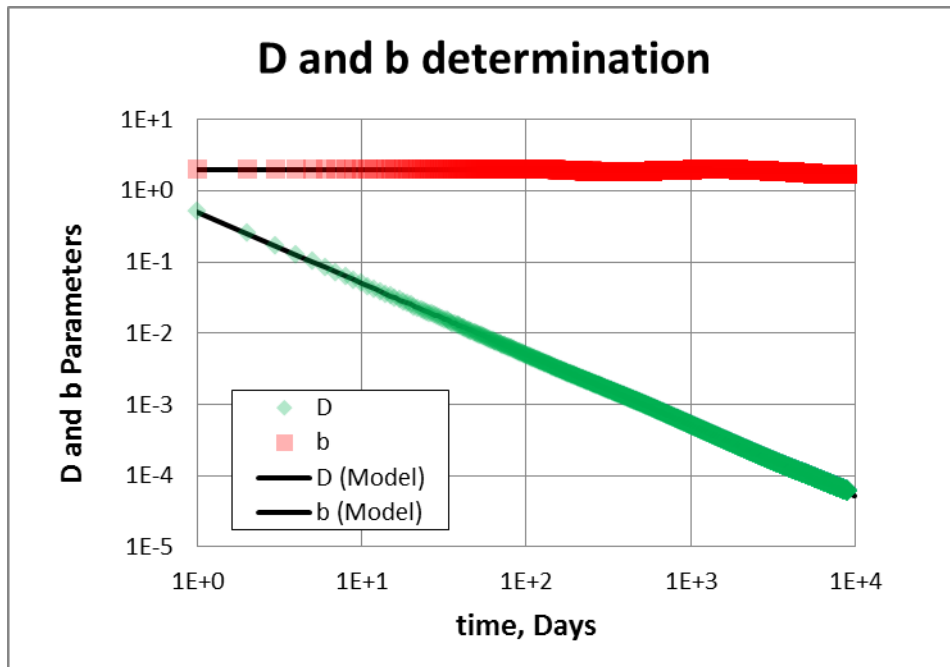


Figure 11. The first matching plot for the PLE method. In this plot, the parameters n , D_1 , and D_∞ are found through iteration.

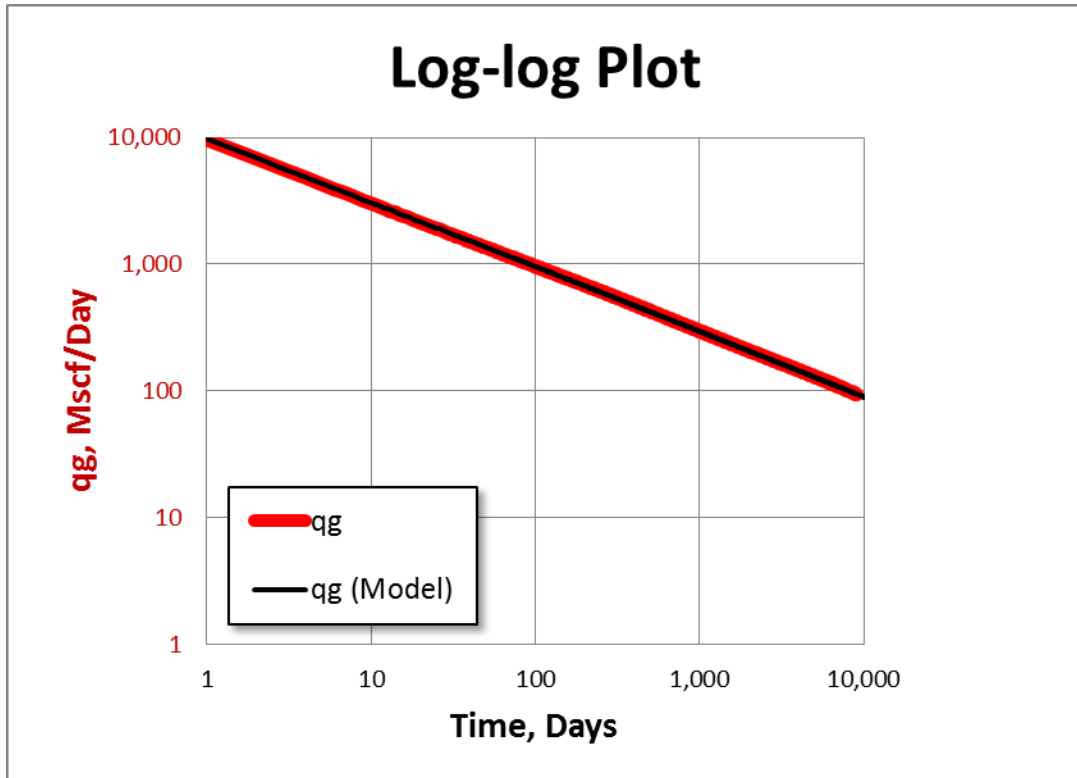


Figure 12. The second matching plot of the PLE method. In this plot, iterations find q_i .

3.3 SEPD Equation Form and Iteration Time Problem

As mentioned in the method review chapter, the SEPD method is mathematically similar to the PLE method. The relationship between the parameter τ and parameters from the PLE method is shown in equation 3.5. However, both methods result in two different matches when non-linear regression is used (Figure 13). This is because of two reasons. The first reason is that the same match can be achieved with a very small-in-magnitude τ which is difficult to find using regression. This is because each iteration step improves on the previous step by a fraction and this process takes a very long time to find the required small-in-magnitude solution.

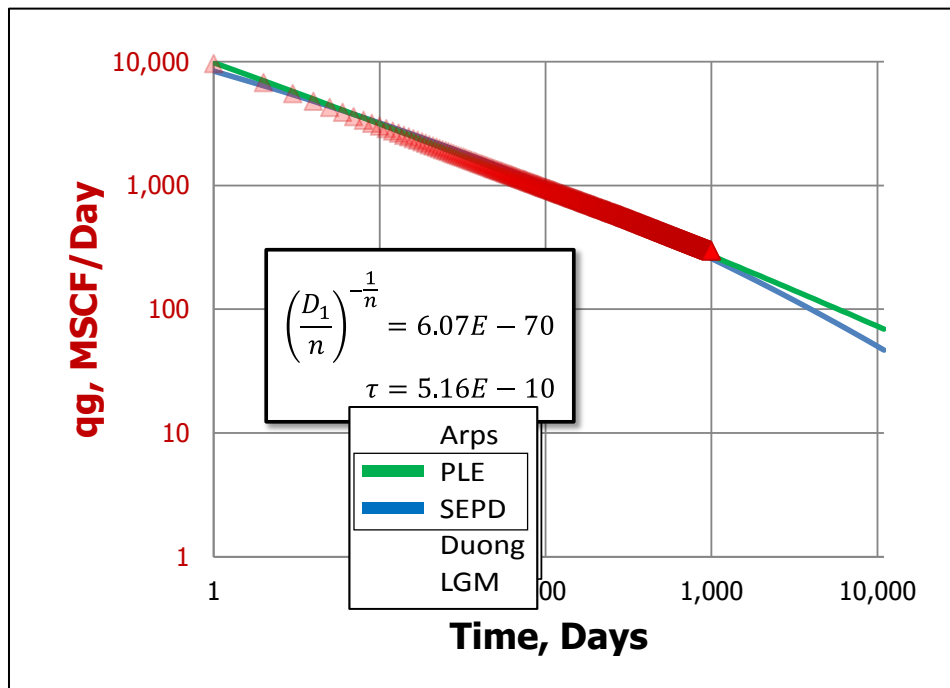


Figure 13. The PLE and SEPD methods with the best match found using iteration. Even though both methods are mathematically similar, iteration finds a better match for the PLE method.

The second reason is that the PLE method finds most parameters by fitting a straight-line in loss-ratio plot. Fitting a straight line is faster than fitting the complicated power-law equation of the SEPD method.

$$\tau = \left(\frac{n}{D_1}\right)^{\frac{1}{n}} \dots\dots\dots (3.5)$$

3.3.1 The SEPD Method and Long Iteration Convergence Time

To overcome the long iteration problem we use the Levenberg-Marquardt Algorithm (LMA) which is faster than Excel Solver. Figure 14 shows a comparison between Excel Solver and LMA. Both methods find similar solutions however the LMA method takes less than half the time Solver takes. The SEPD method is the slowest method to converge compared to the other four methods. A comparison of the convergence time is shown in Figure 15.

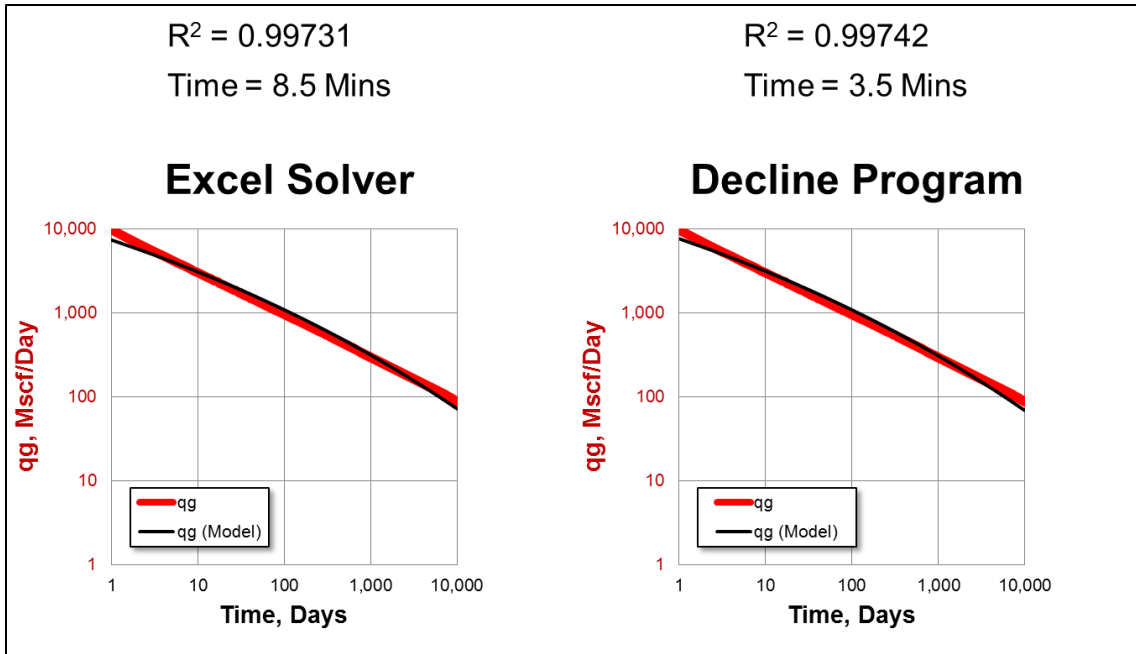


Figure 14. A comparison between Excel Solver and LMA. LMA takes less than half the time Excel Solver takes to find the same solution.

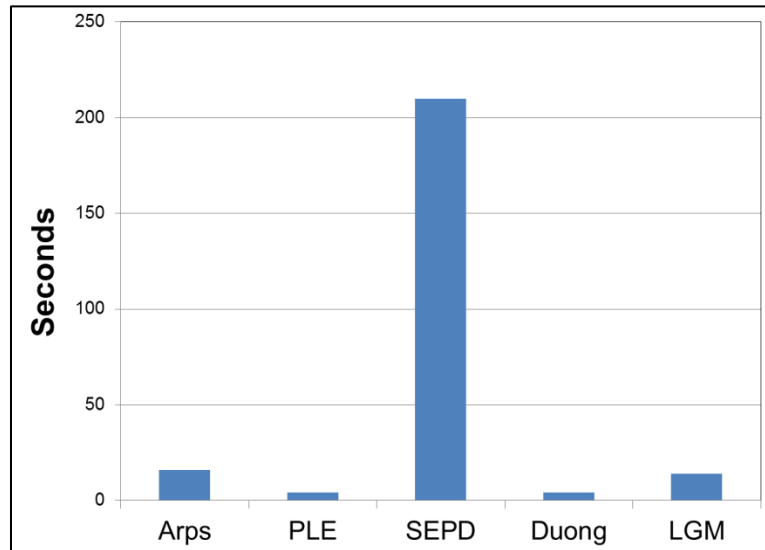


Figure 15. A comparison of convergence time between all five methods. The comparison case is infinite acting linear flow lasting for 30 years.

3.4 Duong's Method Precautions

Duong started deriving his equations from analytical solutions which are based on physical theory. However midway through derivations he changed the analytical equations to empirical ones by adding a fiddle factor (m). The derivation details are shown in Duong's paper and are also derived in Appendix B. Another fiddle factor that Duong used in the final form of the rate-time equation is (q_∞). This term was added to better fit field data. The term, however, might cause problems because Duong explicitly stated in his paper that q_∞ can either be positive or negative.

3.4.1 Duong's q_∞ Error and Improvements

If the term q_∞ is positive, the rate forecast at late production times might actually increase which is not physically possible. Even if a good match is achieved using q_∞ , Duong's cumulative equation does not account for q_∞ and results in wrong cumulatives. Therefore, in this study we recommend using Duong's cumulative equation only when q_∞ is zero. If it is not zero, cumulative should be calculated discretely.

3.4.2 Error in Linear or Bilinear Flow

Duong's method cannot rigorously model linear or bilinear flow. This is because Duong used the fiddle factor (m) which is supposed to be equivalent to 1 for linear or bilinear flow. This can be proven using the relationship between time and material balance time as shown in Figure 16. The problem is that Duong's final form equations are not define at $m=1$. Therefore, a value bigger but as close as possible to 1 should be used instead.

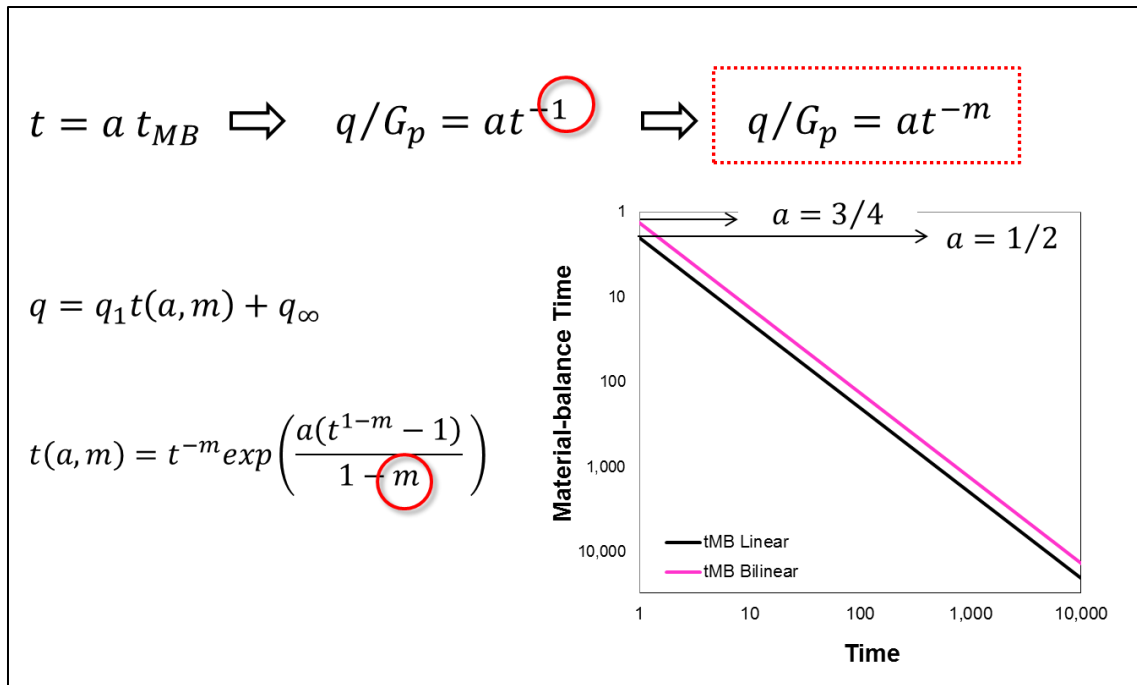


Figure 16. Duong's relationship is actual a relationship between time and material-balance time. Analytical solutions show that m in Duong's equation should be 1. However, substituting $m=1$ in the rate-time relation equation gives an undefined result.

3.4.3 Material-balance Time Error Results in Recovery Underestimation

Material-balance time is defined as the cumulative divided by the last rate (equation 3.6). The cumulative is usually discretely calculated by either using a trapezoidal or a stair-step approximation. This approximation causes errors in t_{MB} for linear or bilinear flow if data is from simulation or analytical solutions. Calculation of the correct material-balance time is significant because Duong's method requires finding the parameter a and m from a plot of time and t_{MB} (Figure 17). In analytical solutions, the calculated rate is an instantaneous rate which changes rapidly in linear or bilinear flow. The first step cumulative in both trapezoidal and stair-step approximation assumes

that rate is constant leading to a wrong material-balance time. Similarly, simulation usually reports rate on a geometric time scale and has an error similar to that of analytical solutions during early times. This study proposes a method to eliminate errors in material-balance time calculations by correcting the first step cumulative (Figure 18). The corrections for cumulative in both linear and bilinear flows are shown below and the effect of t_{MB} error is illustrated in figures (Figure 19). Derivation of the time and material balance time relation is shown in Appendix C.

First step cumulative correction for linear flow,

$$t_{MB} = \frac{Q}{q} \dots\dots\dots (3.6)$$

First step cumulative correction for linear flow,

$$Q_{1st} = 2tq \dots\dots\dots (3.7)$$

First step cumulative correction for bilinear flow,

$$Q_{1st} = \frac{4}{3tq} \dots\dots\dots (3.8)$$

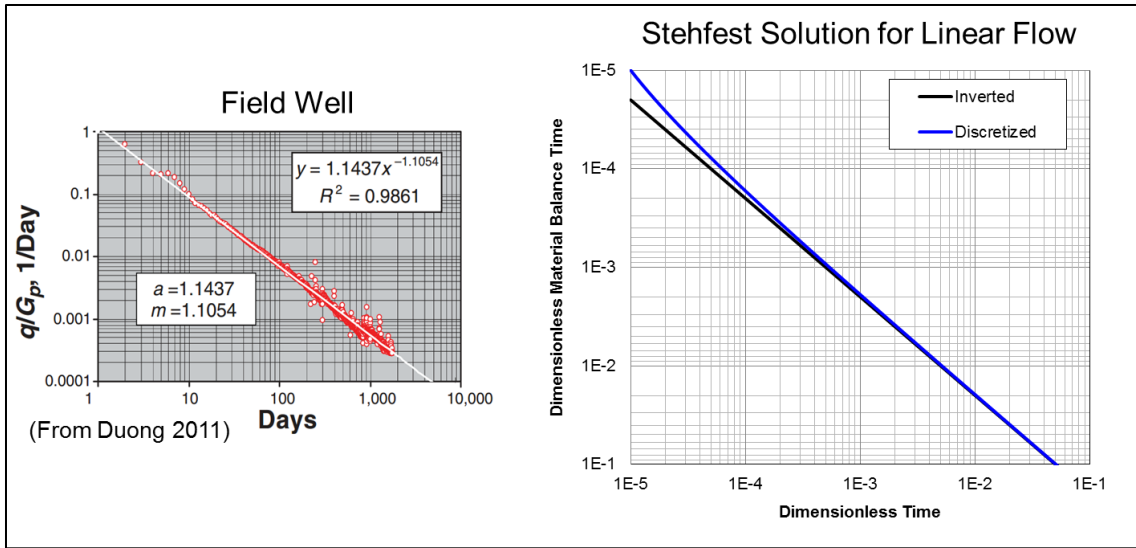


Figure 17. Duong’s method requires finding the parameter a and m from a plot of time and t_{MB} . The error in t_{MB} leads to obtaining wrong values for m .

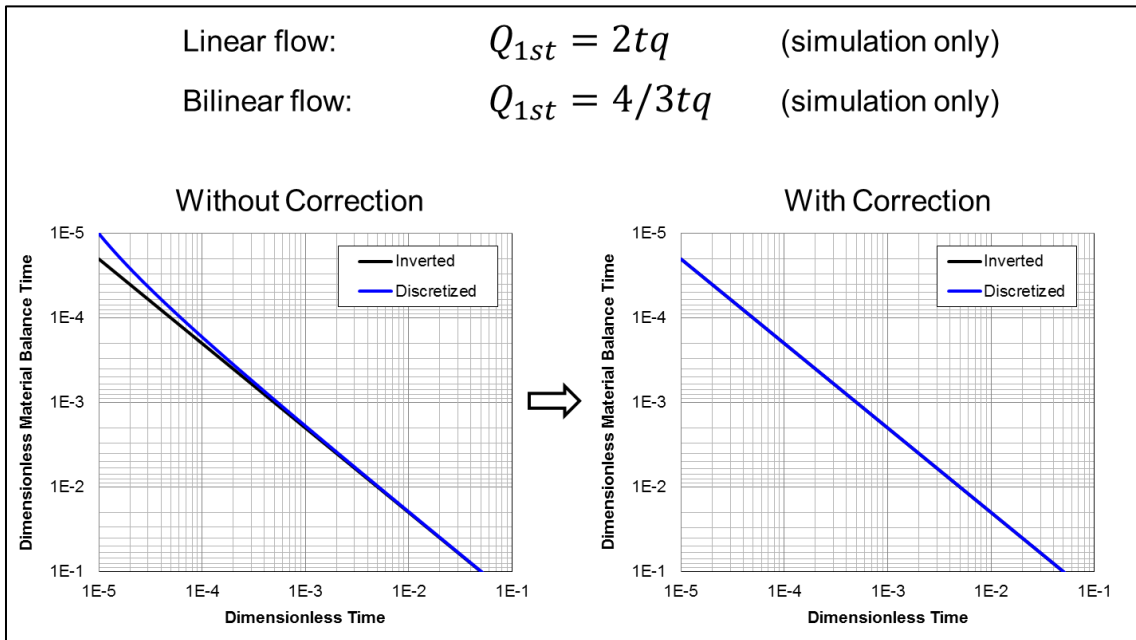


Figure 18. Correction for the first step cumulative eliminates the error in material-balance time.

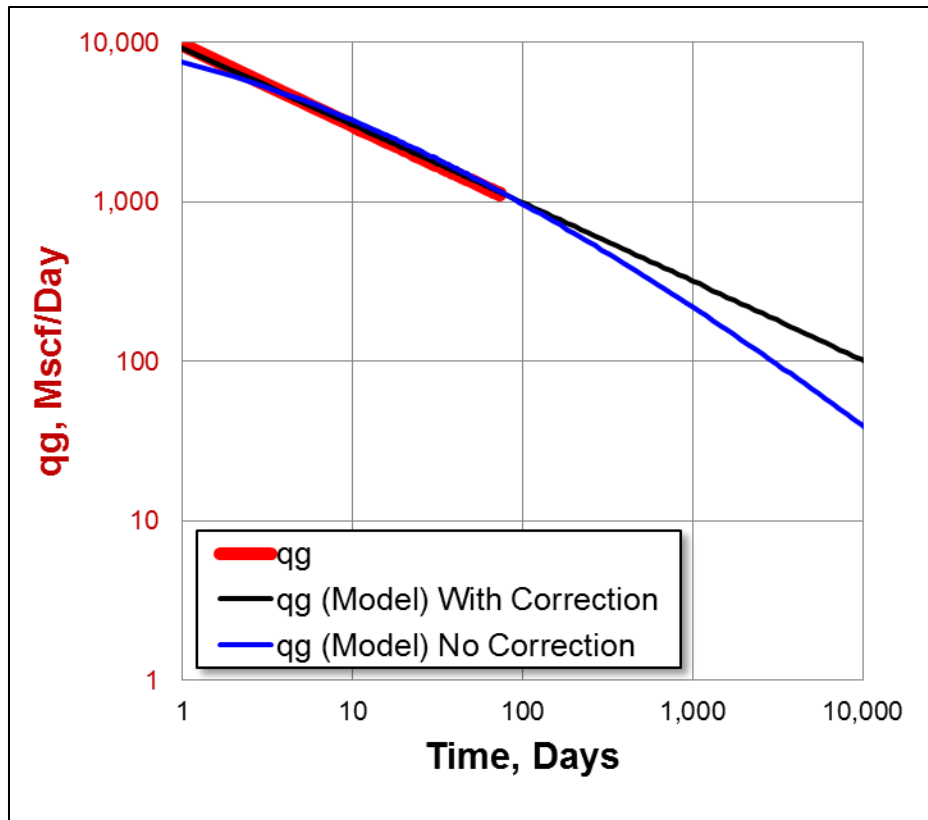


Figure 19. Material-balance time error results in a bad match. Correction for the first step cumulative results in a better match for data. The term q_{∞} was constrained to zero for comparison purposes.

CHAPTER IV

MATCHING AND CALCULATION PROCEDURE

This chapter discusses the matching and calculation procedure used in the Decline program which is developed for this study. The procedure has three main parts: filtering, matching, and EUR calculations.

4.1 Liquid Loading Filter

Field data may have noise due to liquid loading or partial shut-ins. This noise can be filtered out using Turner's methods (Turner et al. 1969). The method calculates the critical rate by using fluid properties at the well head. Any gas flow rate that is less than critical flow rate is filtered out. This filtering process prevents the iteration to be biased by liquid loading data.

Critical velocity for water,

$$v_c(\text{water}) = \frac{5.62 (67 - 0.0031 p)^{0.25}}{(0.0031 p)^{0.5}} \dots\dots\dots (4.1)$$

Critical velocity for condensate,

$$v_c(\text{condensate}) = \frac{4.02 (45 - 0.0031 p)^{0.25}}{(0.0031 p)^{0.5}} \dots\dots\dots (4.2)$$

Critical flow rate in terms of critical velocity

$$q_c \left(\frac{\text{Mscf}}{D} \right) = \frac{3060 p v_c A}{T Z} \dots\dots\dots (4.3)$$

4.2 Matching Data to Model

The objective function is the sum of squares. The errors are calculated in terms of logarithms. This is because data are usually plotted on semi-log or log-log plots which have rates plotted on a log scale y-axis. This allows the regression to find a match that engineers find with simple eyeballing and type curve matching. A weighting factor is also included in the log-log plot to account for the log-scale on the x-axis. The objective function and coefficient of determination for both semi-log and log-log plot is shown below. The objective function is minimized using the Levenberg-Marquardt Algorithm (LMA) which is discussed in Appendix D.

Objective function for a semi-log plot.

$$SS_{err} = \sum_{i=1}^n [\log y_i - \log f(x_i, \beta)]^2 \quad \dots\dots\dots (4.4)$$

Objective function for a log-log plot.

$$SS_{err} = \sum_{i=1}^n w_i [\log y_i - \log f(x_i, \beta)]^2 \quad \dots\dots\dots (4.5)$$

Where the weighting factor is defined as,

$$w_i = \frac{\log \frac{x_{i+1}}{x_i}}{\log \frac{x_{last}}{x_1}} \quad \dots\dots\dots (4.6)$$

The coefficient of determination is defined as,

$$R^2 = 1 - \frac{SS_{err}}{SS_{res}} \quad \dots\dots\dots (4.7)$$

Where the residual for a semi-log plot is defined as,

$$SS_{res} = \sum_{i=1}^n [\log y_i - \bar{y}]^2 \dots\dots\dots (4.8)$$

And the residual for a log-log plot is defined as,

$$SS_{res} = \sum_{i=1}^n w_i [\log y_i - \bar{y}]^2 \dots\dots\dots (4.9)$$

The mean of data is for a semi-log plot is,

$$\bar{y} = \frac{1}{n} \sum_{i=1}^n y_i \dots\dots\dots (4.10)$$

The mean of data is for a log-log plot is,

$$\bar{y} = \frac{1}{n} \sum_{i=1}^n w_i y_i \dots\dots\dots (4.11)$$

4.3 EUR Calculations

The EUR is determined using the following procedure. First, the cumulative at the last reported field data is calculated. Second, the methods are matching to field data. Third, the methods are extrapolated to an economic limit of either rate or time. Forth, reserves are calculated by integrating the area under the extrapolated curves from the last reported field data until abandonment. Finally, the EUR is calculated by adding the last reported cumulative to the reserves (Figure 20).

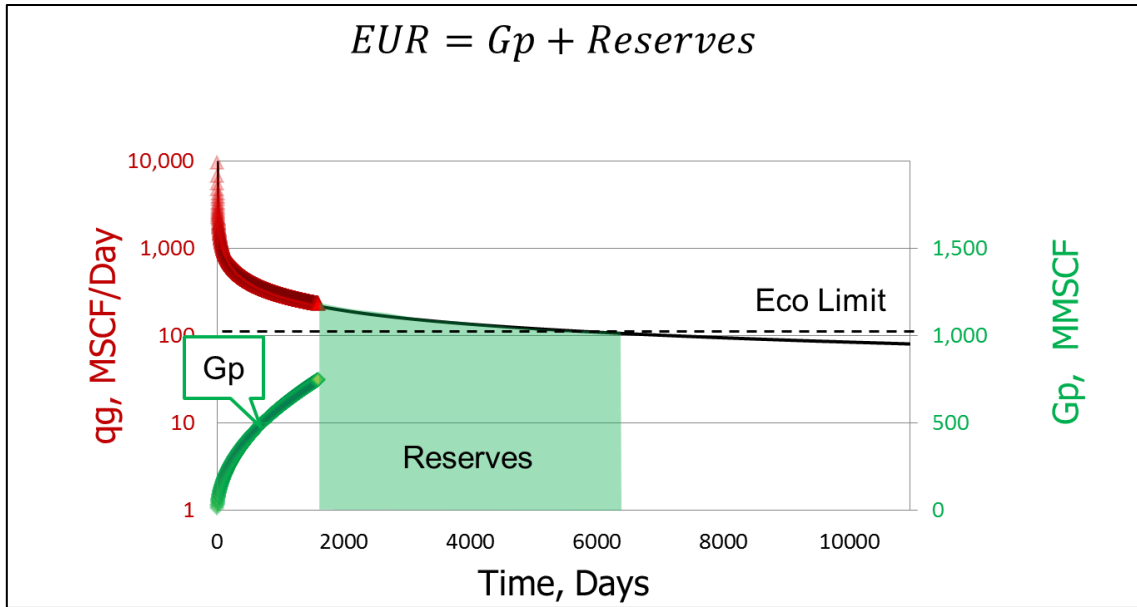


Figure 20. Illustration of procedure to calculate EUR.

CHAPTER V

COMPARISON WITH SIMULATION

5.1 Model Description

Shale wells with multiple traverse hydraulic fractures can be described with two main models: a homogenous model and a naturally fractured model (Figure 21). The former model assumes that fluid flows directly from matrix to hydraulic fractures. The latter model assumes that fluid flows from matrix to hydraulic fractures through natural fractures. Both models have parallel hydraulic fractures and drain a constant stimulated reservoir volume (SRV). In addition to this, natural fractures in the second model are parallel to wells (Ahmadi et al. 2010; Tivayanonda et al. 2012).

There are several ways to visualize fracture distribution in shale wells. The above-mentioned homogenous and naturally fractured models are two possible ways to visualize fractures; however, other models are also possible. Ye et al. (2013) suggested a model in which each hydraulic fracture creates a network (or SRV) that is isolated from others (Figure 22). A model in which hydraulic fractures create an interconnected network is a variation of the model by Ye et al. (Figure 22). All these models result in linear flow which is observed in shale wells, however, this study focus on the homogenous model and naturally fractured model.

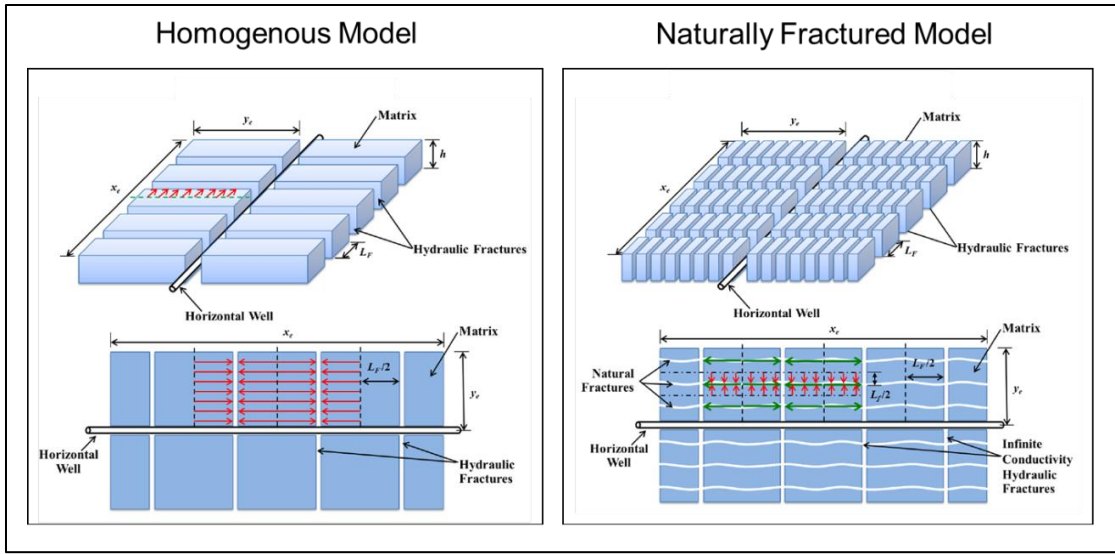


Figure 21. Schematic of the Homogenous Model and Naturally Fractured Model. Both models have parallel hydraulic fractures and assume a constant reservoir volume. The naturally fracture models has also parallel natural fractures that are perpendicular to hydraulic fractures (Tivayanonda et al. 2012).

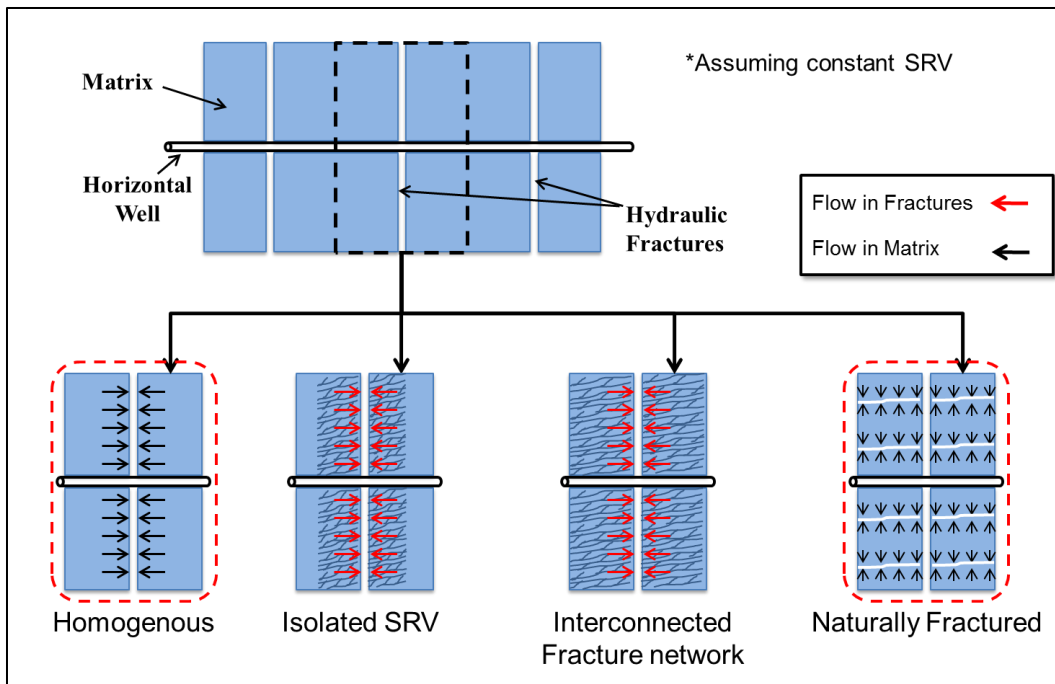


Figure 22. Different ways to visualize fractures in shale wells.

5.2 Simulation and Model Simplifications

The homogenous model and especially the naturally fractured model can be complex. To simplify these models, we adapt two assumptions. The first assumption is that hydraulic fractures have an effectively infinite conductivity. This assumption is reasonable considering that matrix permeability is low compared to hydraulic fracture permeability and would result in four possible declines.

1. Strictly linear flow for the whole production life of the well (Linear).
2. Linear flow followed by BDF (Linear-BDF).
3. Bilinear flow followed by linear flow for the remaining production life (Bilinear-Linear).
4. Bilinear flow followed by linear flow and ending with BDF (Bilinear-Linear-BDF).

Linear flow can occur in both simplified models and is preceded by bilinear flow if natural fractures are present. Linear flow can also be followed by BDF decline if the boundary was reached. However, the BDF might not occur during the economic production life if matrix permeability is too low.

The second assumption that we make is that wells have equally spaced hydraulic fractures and natural fractures. This assumption results in symmetry. Because of that, it is possible to use data tricks and simulate one segment only which makes simulation faster and easier. A detailed schematics showing the symmetry of the models and the simulated segments is shown in (Figure 23) and the resulted four declines are shown in (Figure 24-Figure 27). Simulations are run for 30 years and results are reported in days.

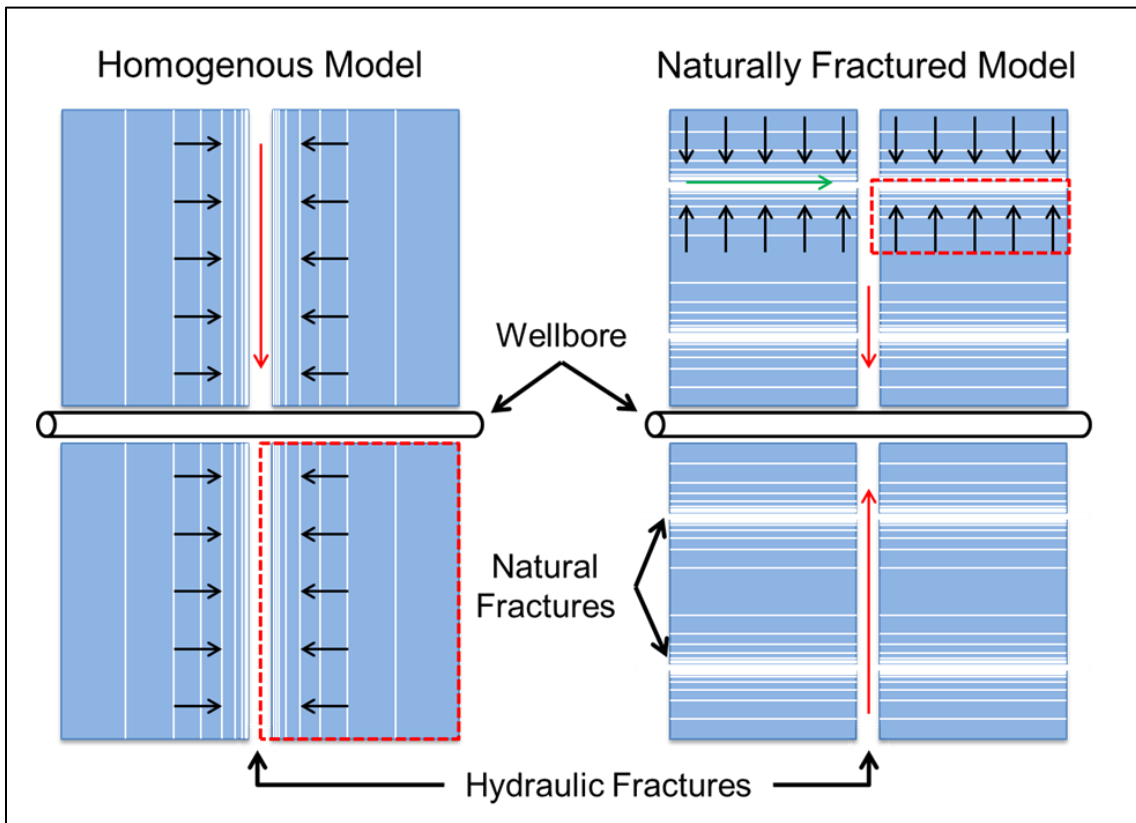


Figure 23. Detailed schematics showing the homogenous and naturally fractured model as well as the simulated segments.

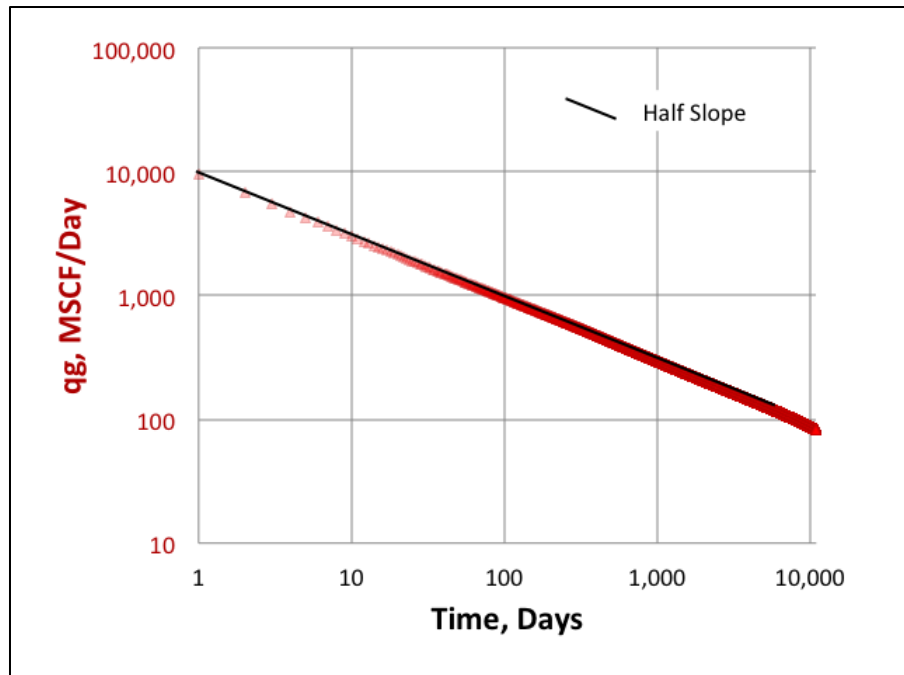


Figure 24. Case 1: infinite acting linear flow until abandonment.

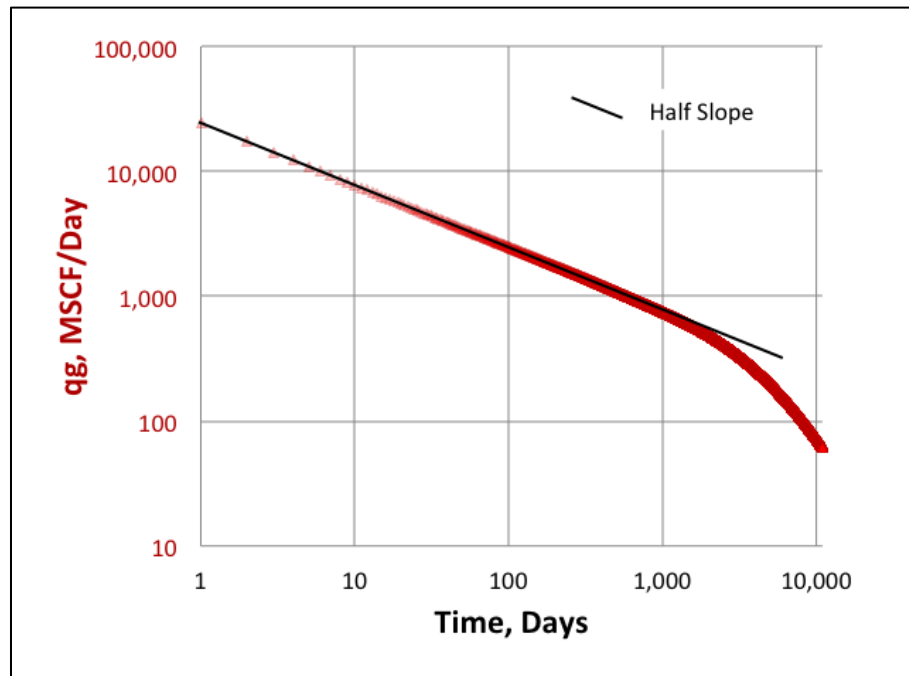


Figure 25. Case 2: linear flow following by boundary dominated flow at around 1000 days.

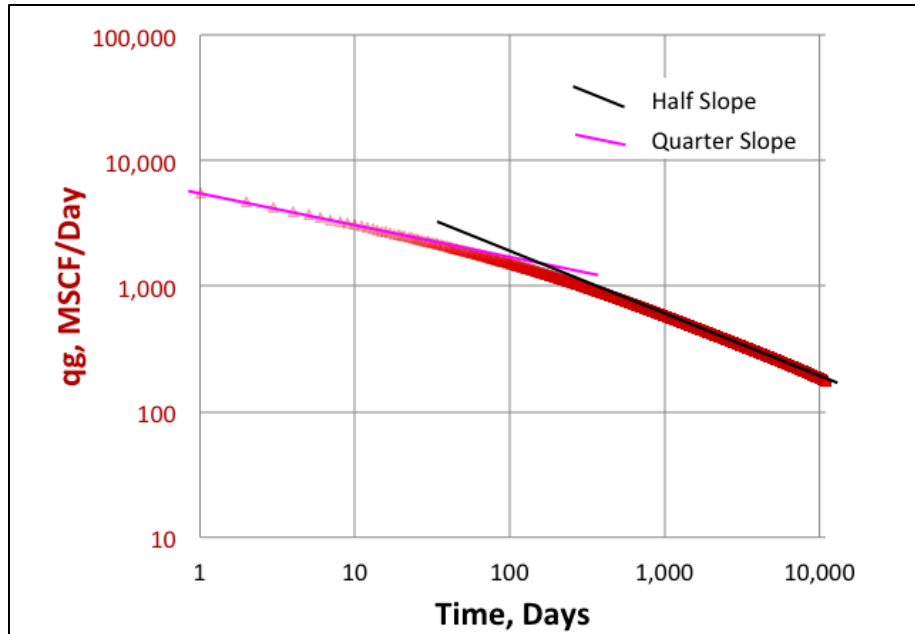


Figure 26. Case 3: Bilinear flow followed by linear flow which lasts until abandonment.

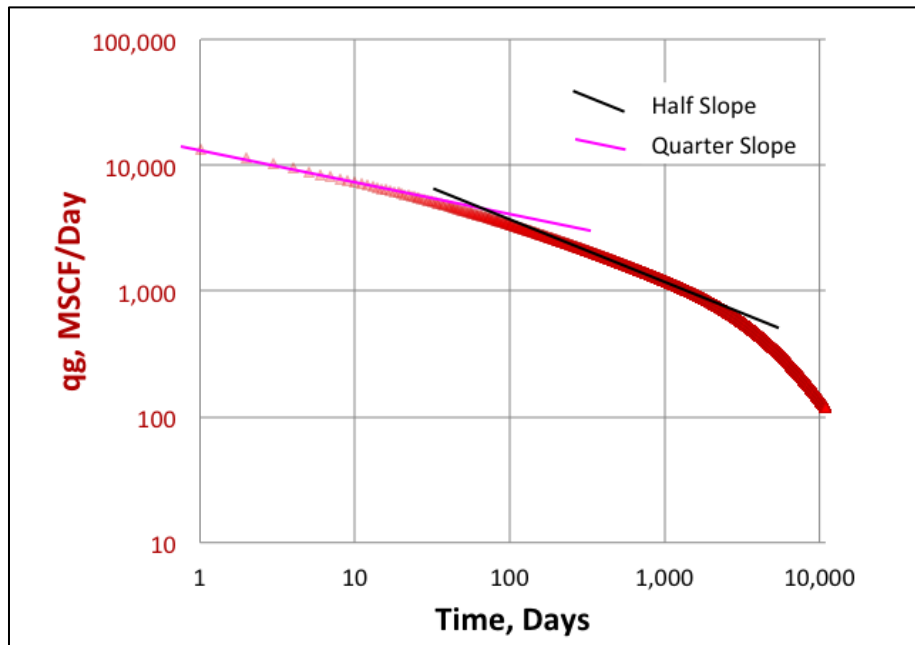


Figure 27. Case 4: The case has all three flow regimes. Bilinear then linear then BDF.

5.3 Matching Methods to Simulation: A Decline Fit Comparison

The objective of this section is to evaluate whether the different decline curve methods can match simulation. The four simulated cases shown in the previous section are used as test cases.

5.3.1 Case 1 – Linear Flow

Figure 24 shows the simulated production for case 1. A linear flow half-slope is observed until abandonment at 30 years. The best fit for each of the methods is shown in Figure 28 to Figure 32. All methods can be reasonably shaped into straight-lines to model case 1 except for the SEPD method which tends to curve. Nonetheless, forcing the SEPD model into a straight line is possible since it is mathematically identical to the PLE model. For case 1, the equivalent τ that makes the SEPD model identical to the PLE is ($\tau = 8.2E - 69$). This value is very small and outside the iteration sensitivity range and therefore this solution was not found. The Arps model was shaped into a straight line using a relatively large D and b value of ($b = 2$).

5.3.2 Case 2 – Linear-BDF

This case is similar to case 1 except it shows BDF in the last log cycle (Figure 25). The method comparison (Figure 28 - Figure 32) shows that most methods cannot model case 2 except for the PLE method. Arps' and Duong's methods are not flexible to match both linear and BDF. The LGM and SEPD methods accomplish a reasonable fit for the early part of data but not for late data. The PLE method is the best by reasonably fitting linear and BDF. The PLE method captures the decline shape but it is matching slightly

over the linear flow line. The Duong's method accomplishes a fair match to the BDF period by compromising on early match. Duong's method shows a shape similar to fracture fluid clean up. This is because the m value is higher than 1 and Duong's method curves as m increases (see Duong's type curves.)

5.3.3 Case 3 – Bilinear-Linear Flow

Case 3 shows bilinear flow prior to a long linear flow extending to abandonment (Figure 26). The method comparison (Figure 28 - Figure 32) shows that all methods can reasonably fit this case. The best fit is by the SEPD method. The other methods accomplish reasonable fits by compromising on early or late portion of data.

5.3.4 Case 4 – Bilinear-Linear-BDF

This case is similar to case 3 except it shows BDF in the last log cycle. The simulated production (Figure 27) shows a quarter slope bilinear flow followed by a half slope linear flow and then BDF. Figure 28 to Figure 32 show the method comparison. This case is difficult to match because it has three distinct flow regimes. The best fit is accomplished by the PLE method. The Duong method behaves in a fashion similar to case 2.

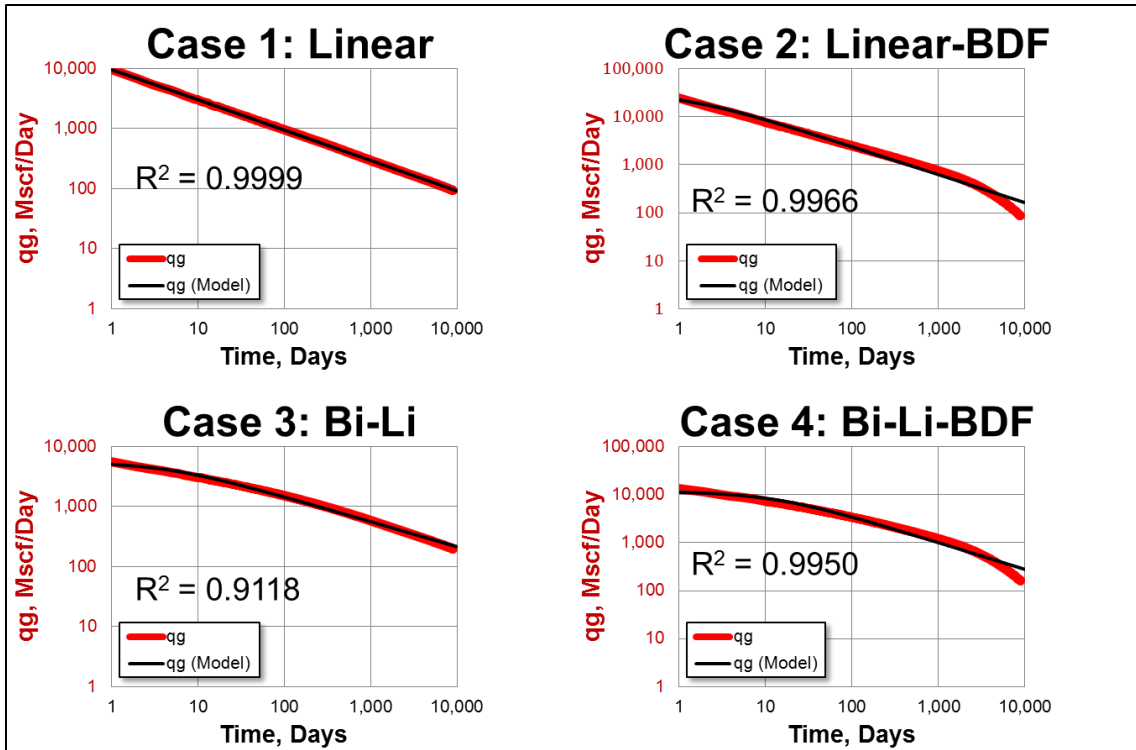


Figure 28. The final iteration match for the Arps Method. Arps Fit Case 1 Perfectly. Arps' method does not fit the other cases accurately because it cannot model multiple flow regimes.

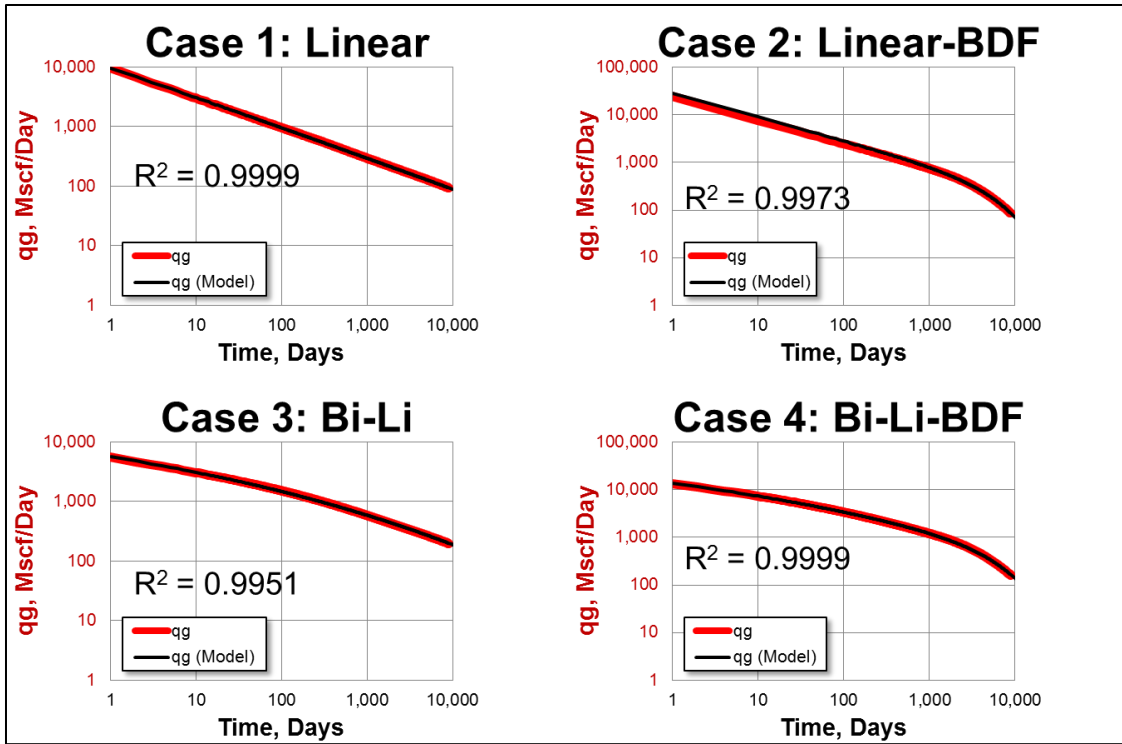


Figure 29. The final iteration match for the PLE method. The PLE method fits Case 1 perfectly and fairly fits Case 2 and 4. Case 3, however, is fitted by coincidence here and might not fit other scenarios similar to case 3 as accurately.

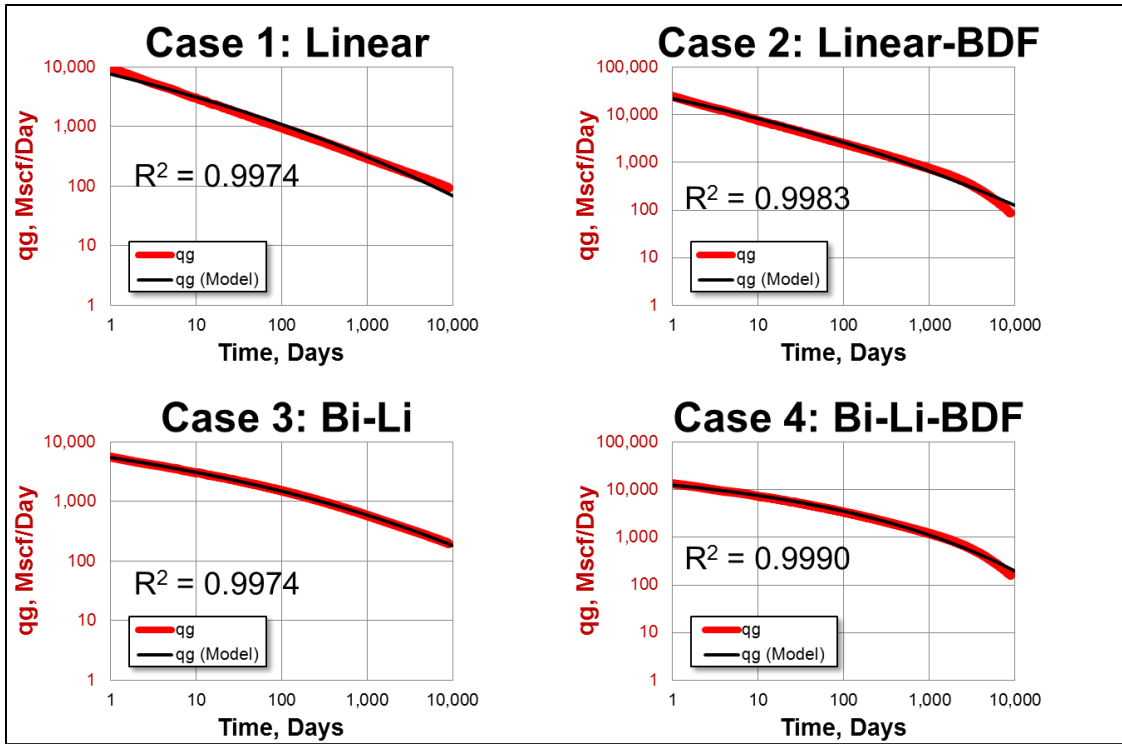


Figure 30. The final iteration match for the SEPD method. The sped method fits gives a good coefficient of determination in most cases however it does not capture the shape. Case 2 is the only case where the method captures the shape.

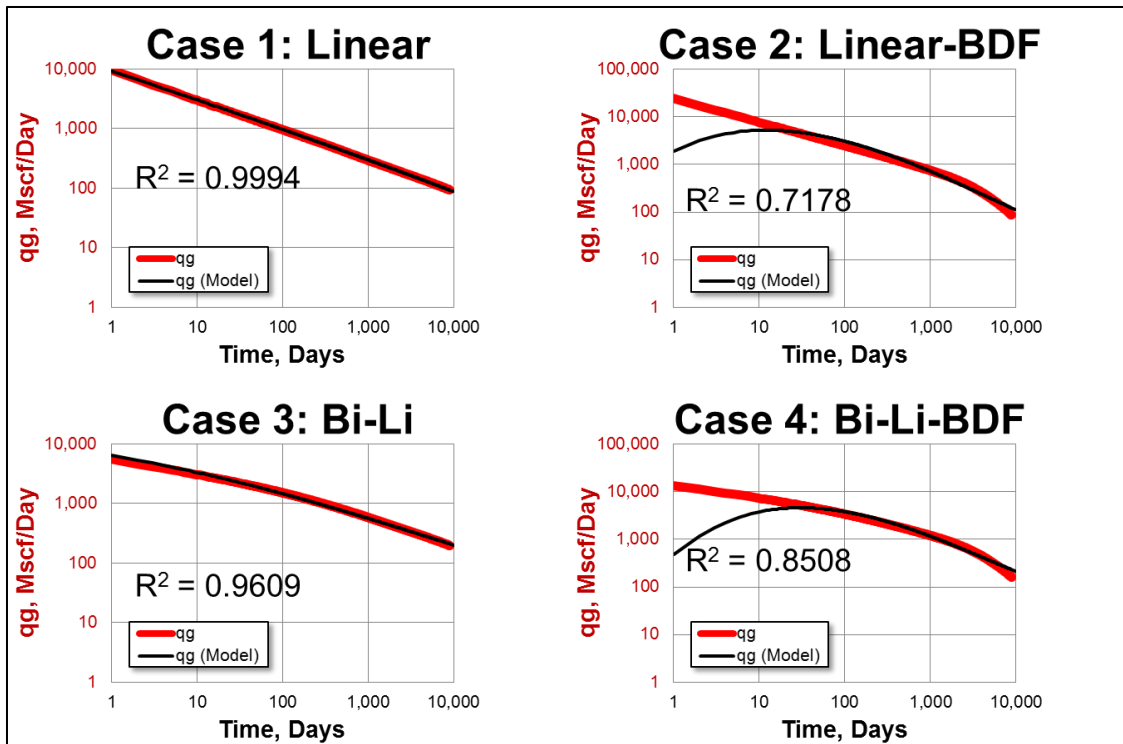


Figure 31. The final iteration match for the Duong method. Does method fairly captures the shape of Case 1 and 3. The other cases are poorly matched.

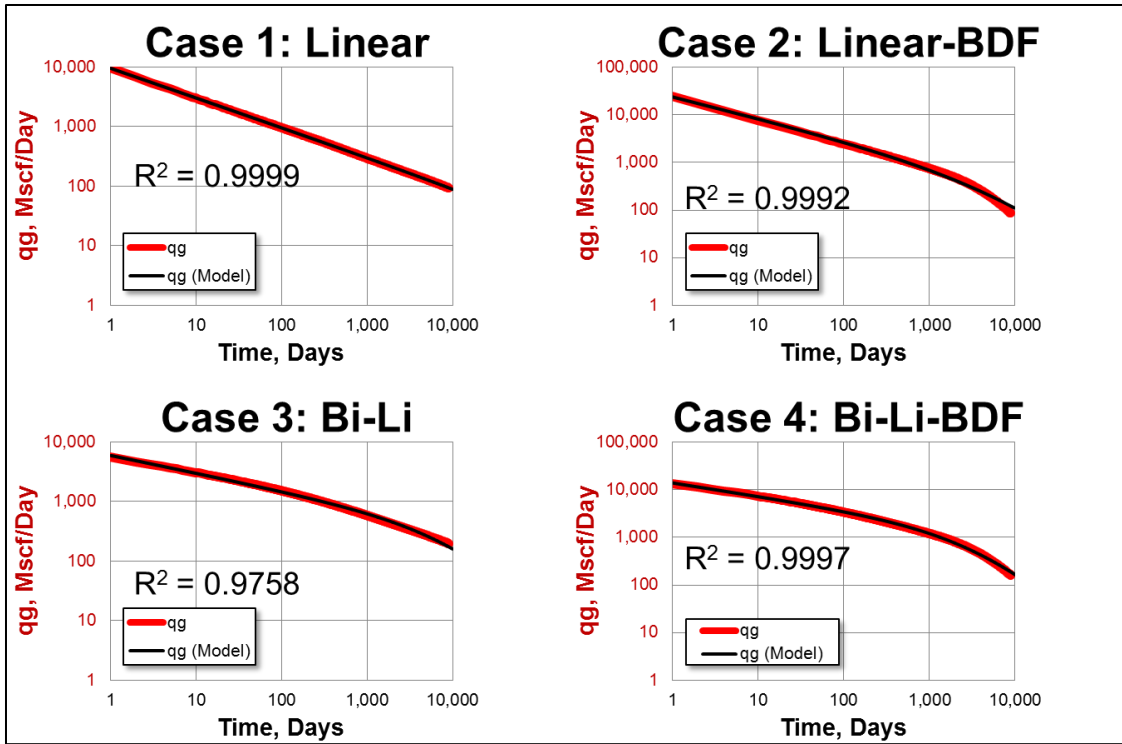


Figure 32. The final iteration match for the LGM method. The method goods good fit and curve shapes however it does not capture the shape of BDF.

5.4 Effect of Production Time on Forecast

The objective of this section is to evaluate the effect of production time on the methods. Data from the four simulated declines are cut at different production times and forecasted using all methods.

5.4.1 Case 1 – Linear Flow

In this case at only 100 days of production (Figure 33), Arps' LGM and PLE method extrapolate linearly and forecast the correct recovery. The SEPD and Duong's methods curve down and forecast the wrong recovery. As production time increases the methods gradually improve until they converge at 9000 days of production (Figure 34- Figure 35). The curving in Duong's method is due to q_{∞} . If the term q_{∞} is constrained to zero, a straight-line forecast is obtained.

5.4.2 Case 2 – Linear-BDF

For case 2 at times prior to BDF decline the methods behave in a similar fashion to Case 1 (Figure 36). However, in this case none of the methods forecast the correct production because the start of BDF decline is unknown from production data alone. At 3000 days, when BDF decline starts, the PLE method is the only method which forecast the correct recovery (Figure 37). At 9000 days the other methods improve in their forecast however they still over estimate recovery (Figure 38).

5.4.3 Case 3 – Bilinear-Linear Flow

At early production times none of the methods forecast the correct recovery of case 3 (Figure 39). However, at 1000 days of production when bilinear flow has ended and linear flow is well established the forecast improves and the true recovery is given by the PLE, SEPD, and Duong's methods (Figure 40). The LGM method still underestimates while the Arps' method still overestimates recovery. At 9000 days of production all methods converge (Figure 41).

5.4.4 Case 4 – Bilinear-Linear-BDF

For case 4 at times prior to BDF decline the methods behave in a similar fashion to Case 3. However, in this case none of the methods forecast the true production even when linear flow is established at 1000 days because the start of BDF decline is unknown from production data alone (Figure 42). At 3000 days, when BDF decline starts, the PLE method is the only method which forecast the true recovery (Figure 43). At 9000 days the other methods improve in their forecast however they still over estimate recovery (Figure 44).

Case 1 – Linear Case

- Forecast at 100 Days of Production

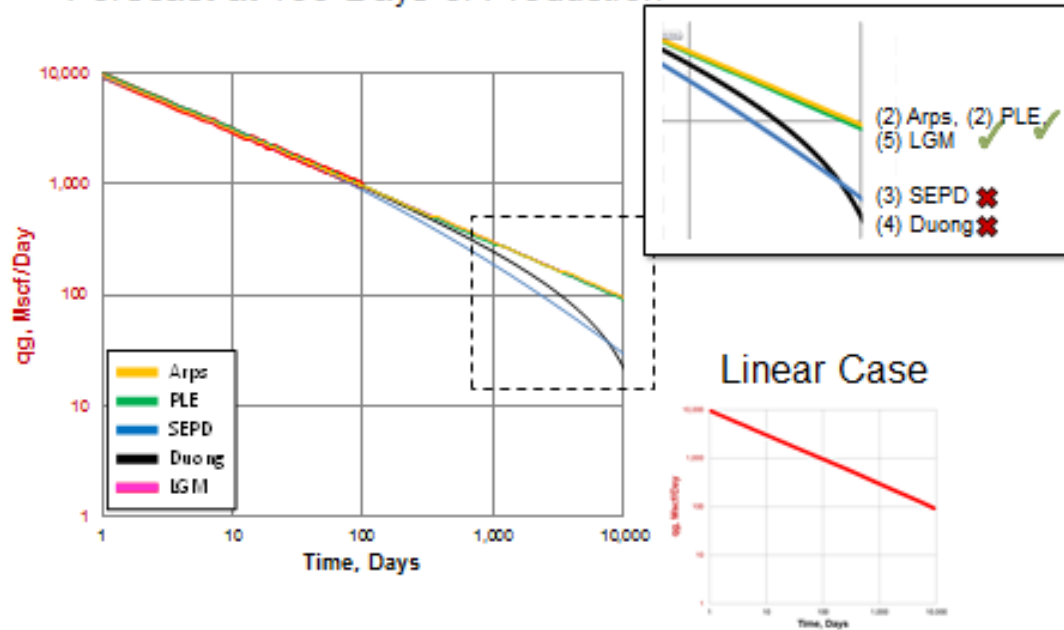


Figure 33. Case 1 forecast comparison with 100 days of production data.

Case 1 – Linear Case

- Forecast at 1000 Days of Production

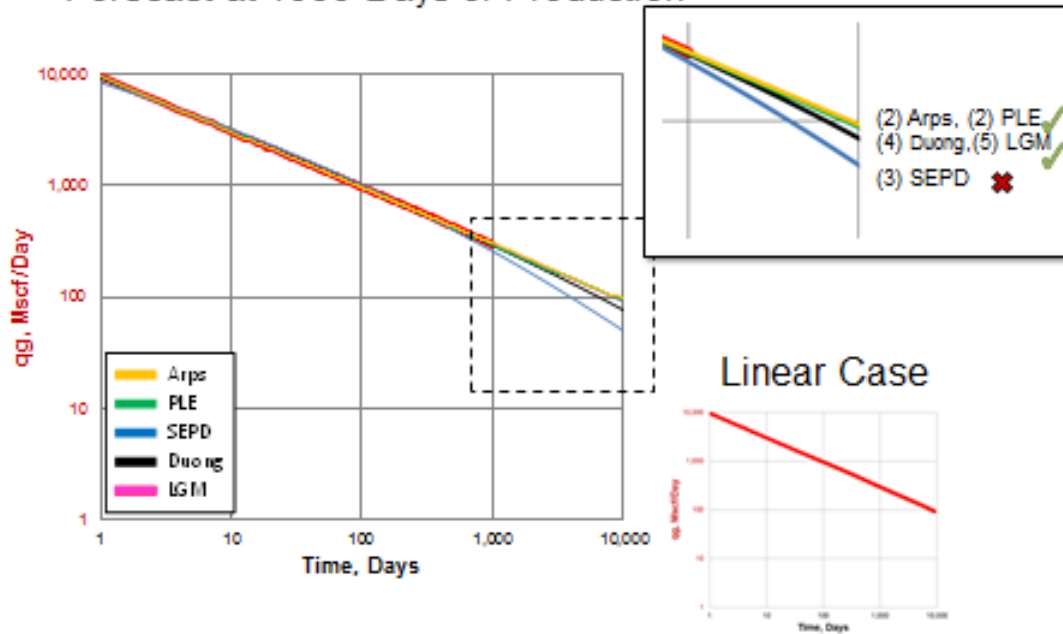


Figure 34. Case 1 forecast comparison with 1000 days of production data.

Case 1 – Linear Case

- Forecast at 9000 Days of Production

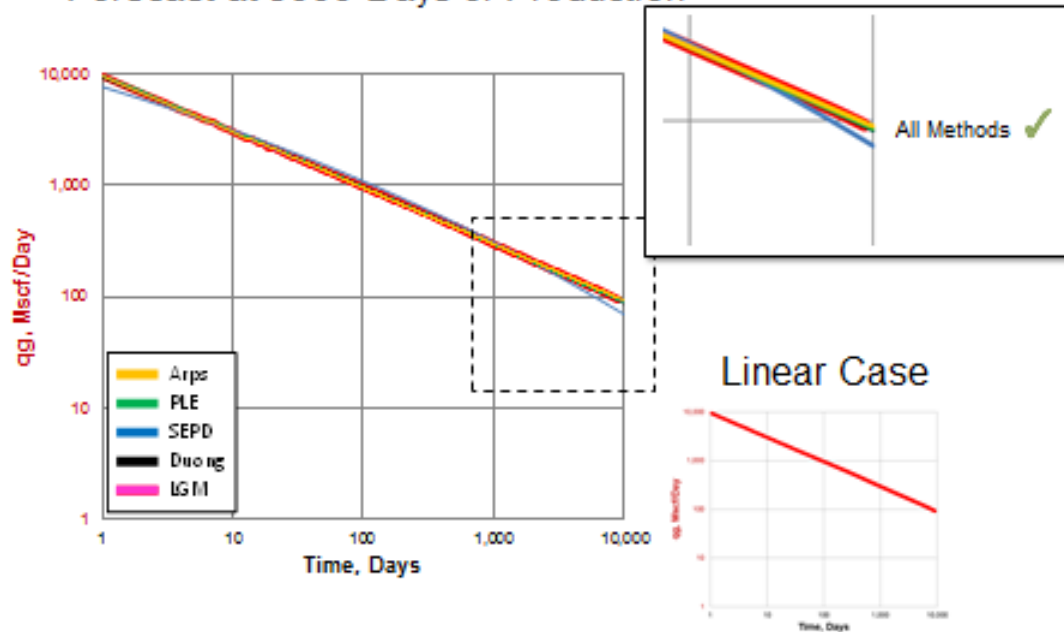


Figure 35. Case 1 forecast comparison with 9000 days for production data.

Case 2 – Linear-BDF

- Forecast at 1000 Days of Production

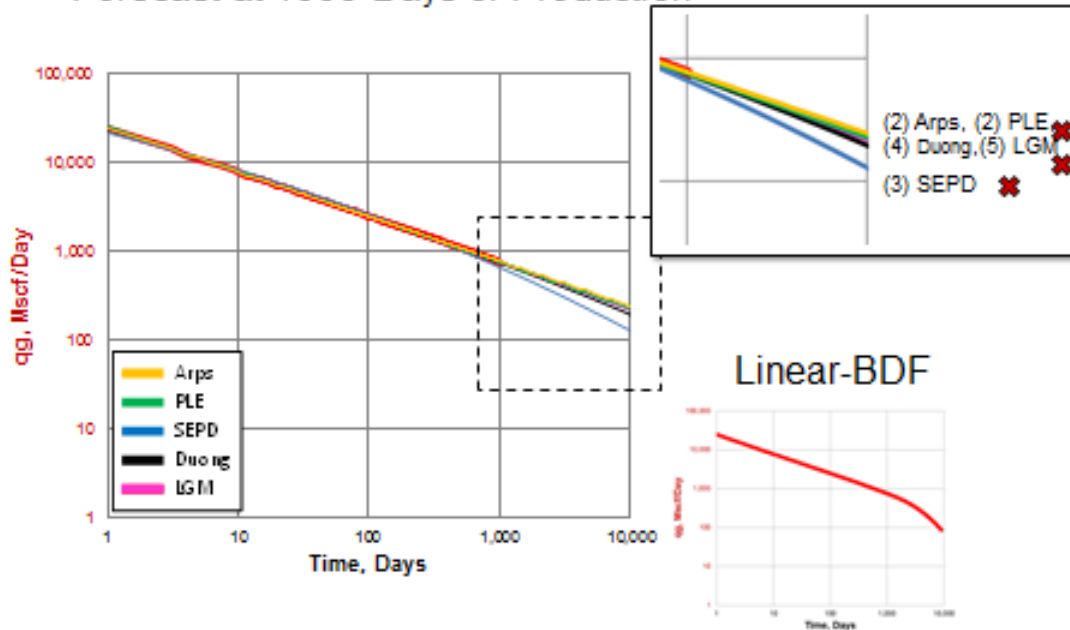


Figure 36. Case 2 forecasts comparison with 1000 days of production data. All methods forecast the wrong production because during transient flow the time of BDF decline cannot be determined with production data alone.

Case 2 – Linear-BDF

- Forecast at 3000 Days of Production

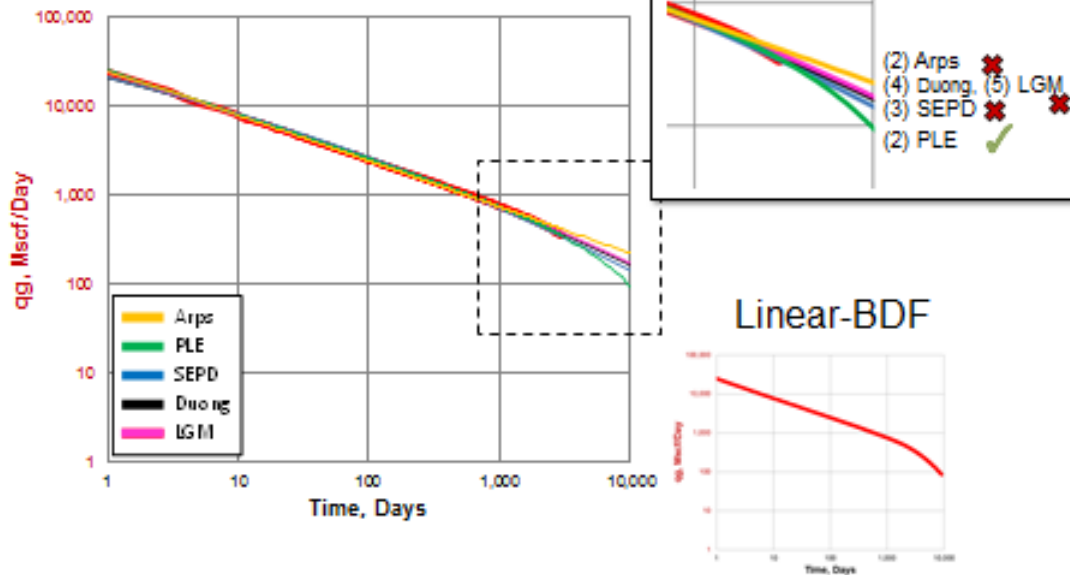


Figure 37. Case 2 forecast comparison with 3000 days of production data. The PLE method is the only method that captures the decline and forecast a correct recovery.

Case 2 – Linear-BDF

- Forecast at 9000 Days of Production

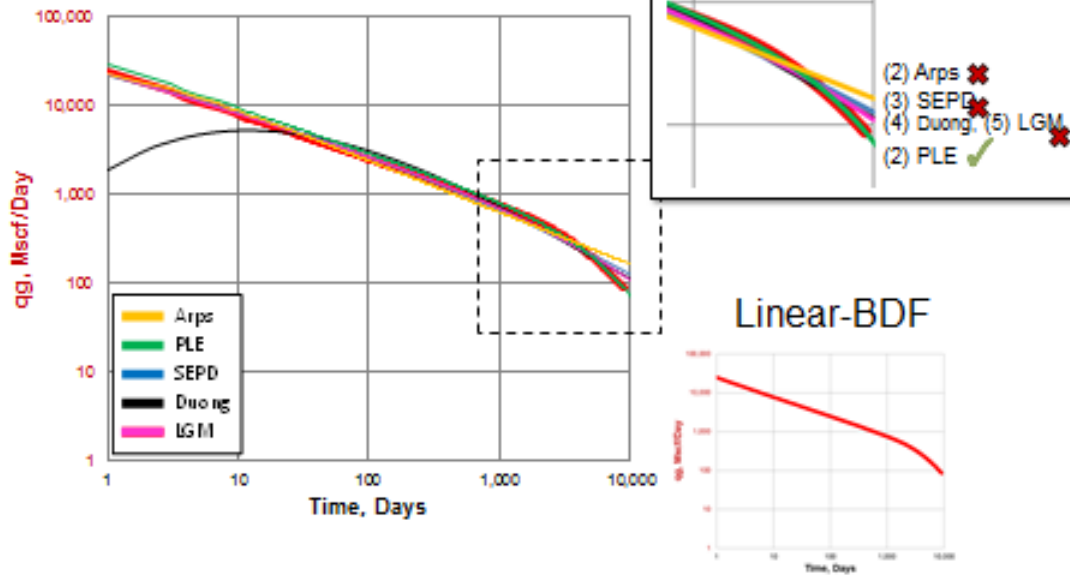


Figure 38. Case 2 forecast comparison with 9000 days of production data.

Case 3 –Bilinear-Linear

- Forecast at 100 Days of Production

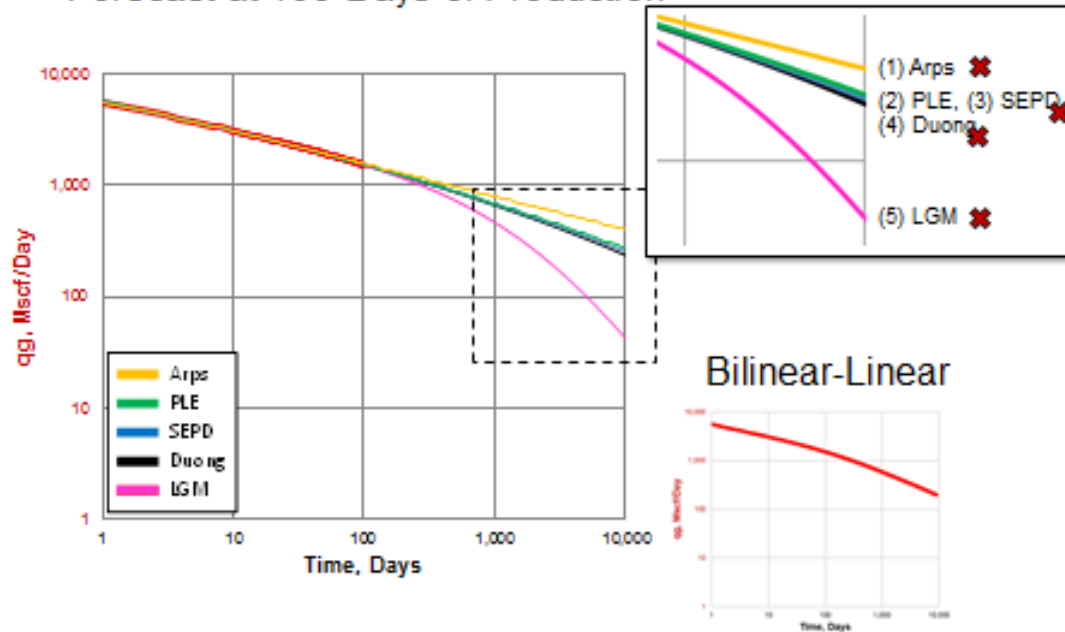


Figure 39. Case 3 forecast comparison with 100 days of production data. None of the methods can forecast the correct production at such early production time.

Case 3 –Bilinear-Linear

- Forecast at 1000 Days of Production

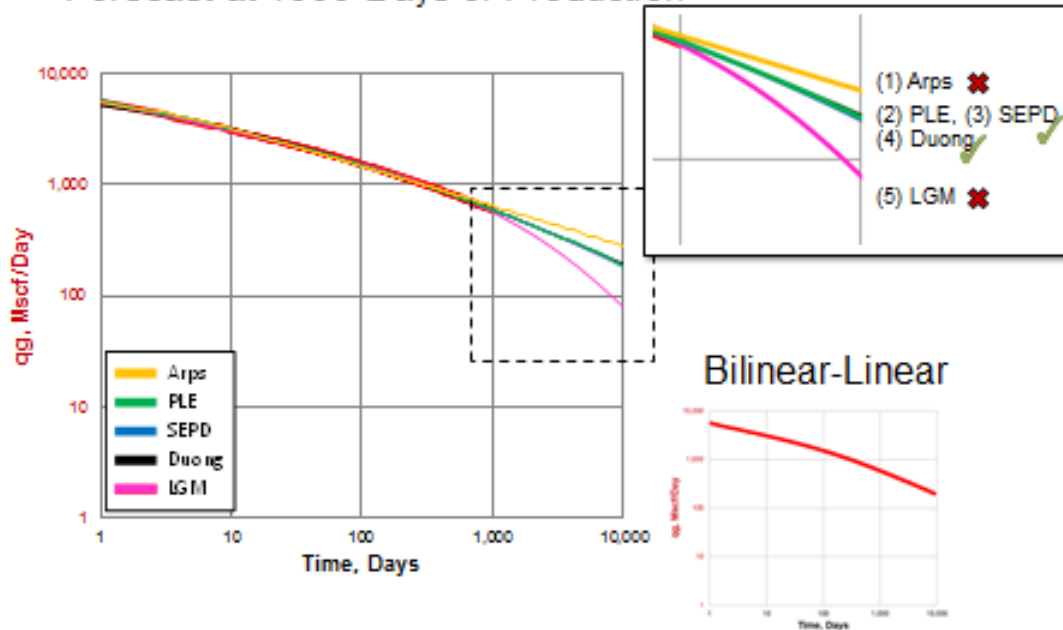


Figure 40. Case 3 forecast comparison with 1000 days of production data. The Arps method overestimates recovery while the LGM Method underestimates. The other three methods forecast production accurately.

Case 3 –Bilinear-Linear

- Forecast at 9000 Days of Production

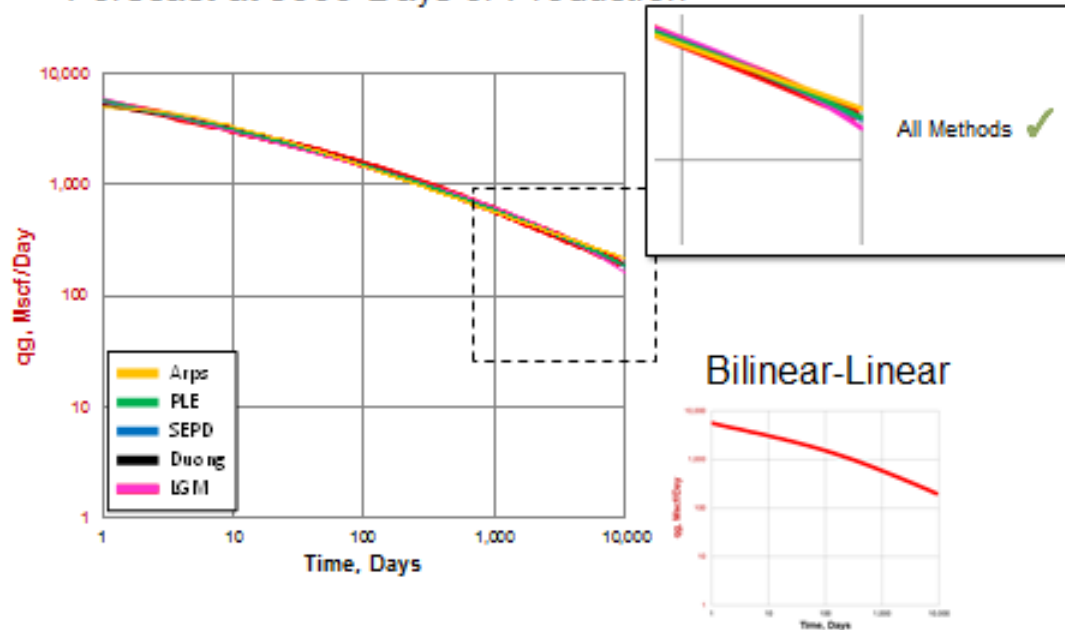


Figure 41. Case 3 forecast comparison with 9000 days of production data. All methods converge at the true match except Arps which is slightly overestimating.

Case 4 – Bilinear-Linear-BDF

- Forecast at 1000 Days of Production

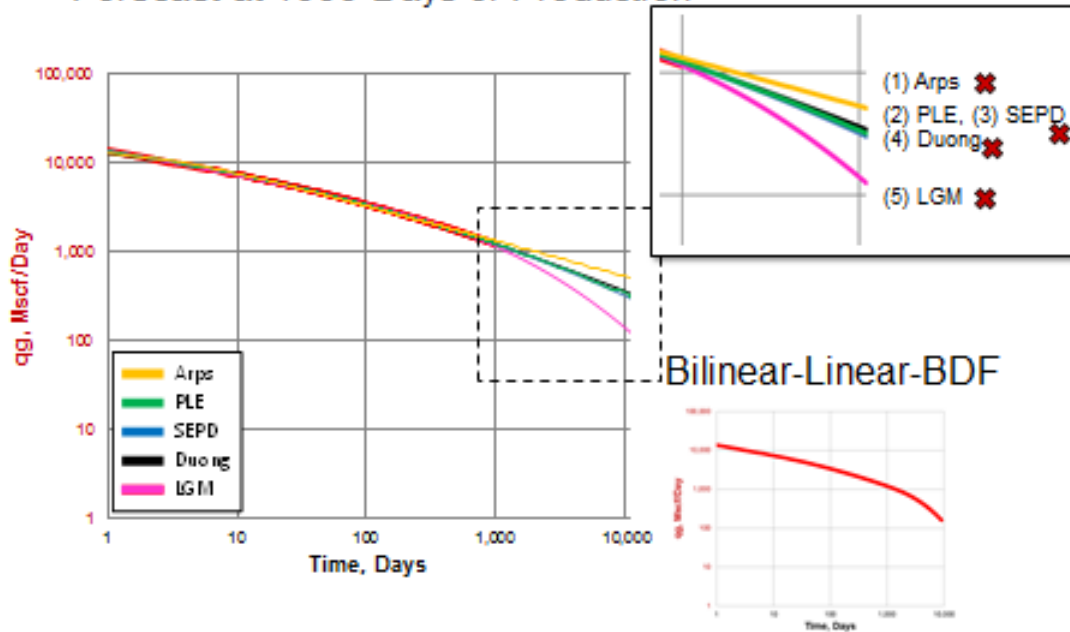


Figure 42. Case 4 forecast comparison with 1000 days of production data. None of the methods forecast the true production because the time of BDF decline cannot be determined with production data alone.

Case 4 – Bilinear-Linear-BDF

- Forecast at 3000 Days of Production

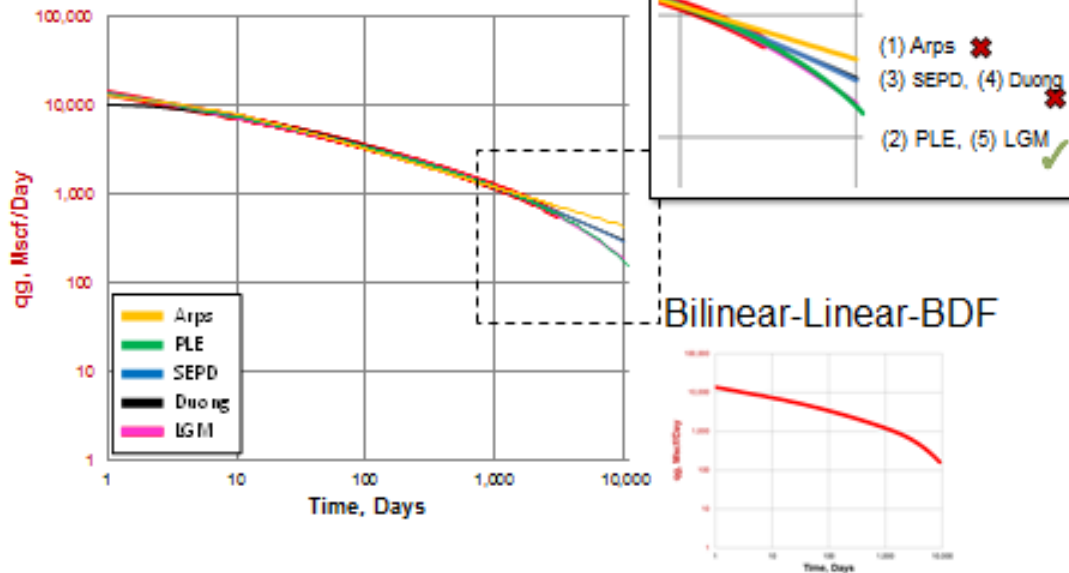


Figure 43. Case 4 forecast comparison with 3000 days of production. The PLE and LGM methods capture the true profile.

Case 4 – Bilinear-Linear-BDF

- Forecast at 9000 Days of Production

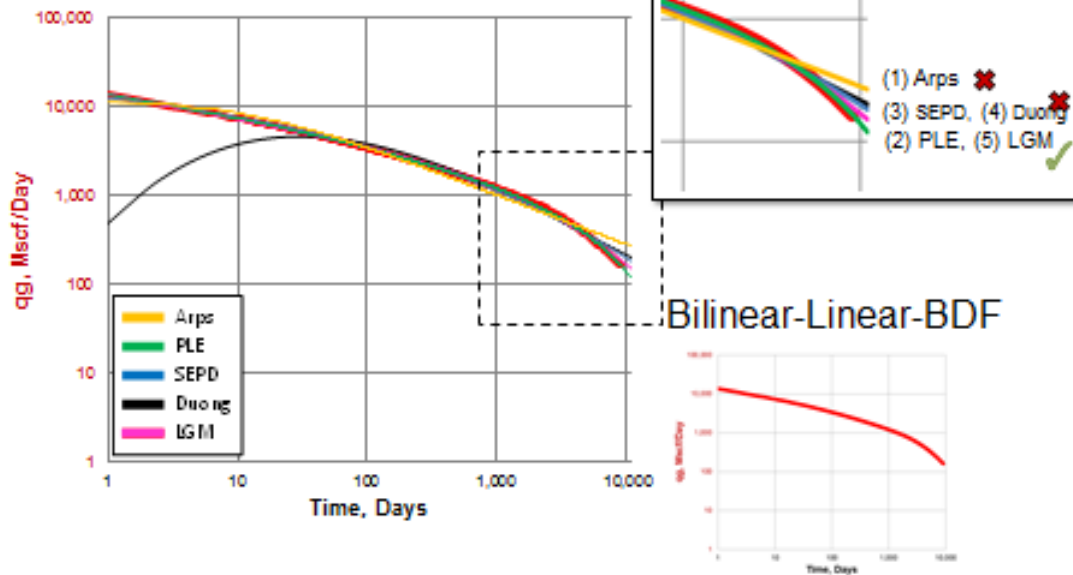


Figure 44. Case 4 forecast comparison with 9000 days of production. The PLE and LGM are still the best. The other methods slightly overestimate recovery.

CHAPTER VI

FIELD EXAMPLES

The different decline methods were applied to 4 wells from different fields. These fields are the Barnett, Bakken, Eagleford, and Fayetteville fields.

6.1 Barnett Shale Gas - Well B-314

Well B-314 is a shale gas well from the Barnett shale. The well shows linear flow half-slope followed by a deviation that can be considered as BDF (Figure 45). At long production times some rates fall short from the linear flow half-slope trend. These lower rates are caused by either liquid loading or partial shut-ins. These rates are filtered out using Turner's method.

The forecast and EUR is shown in Figure 45. This case is similar to Case 4 and the PLE should be the most accurate method while the other methods should improve with production time. The LGM and SEPD methods give forecasts similar to the PLE. The Duong method is overestimating because production time of BDF decline is not sufficient.

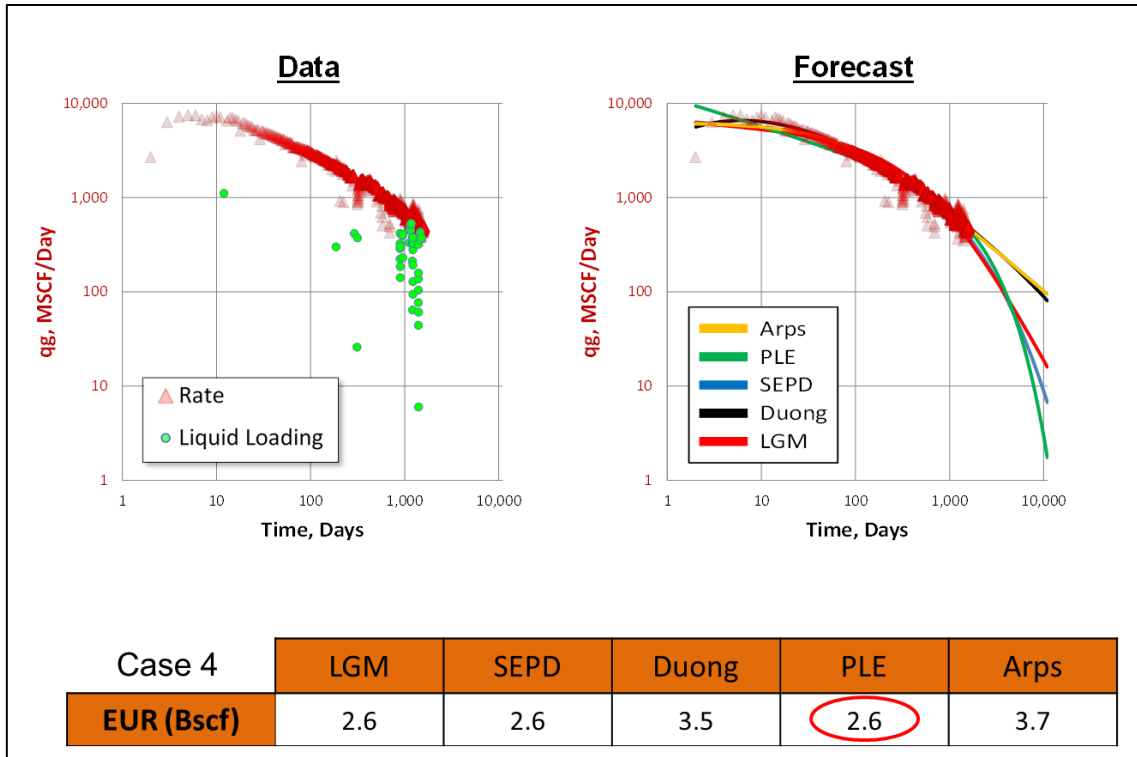


Figure 45. Barnet Well B-314. The well exhibits linear flow and BDF. The best method when BDF is reached is the PLE method. The other methods should converge as production time increase.

6.2 Bakken Shale Oil - Well BK-86

Well BK-86 is an oil well from the Bakken shale. Its production shows a half-slope indicating transient linear flow to 875 days and the forecast is shown in Figure 46. Noisy data are removed manually to improve matching. This well is in transient linear flow and it might either continue showing linear flow until abandonment (Case 1) or go into BDF if boundary is reached (Case 2). For case 1 the Arps, LGM and PLE method should result in good forecasts. However, in this well the SEPD method also gives a similar forecast. For Case 2, the forecast has to be rerun when the boundary is reached.

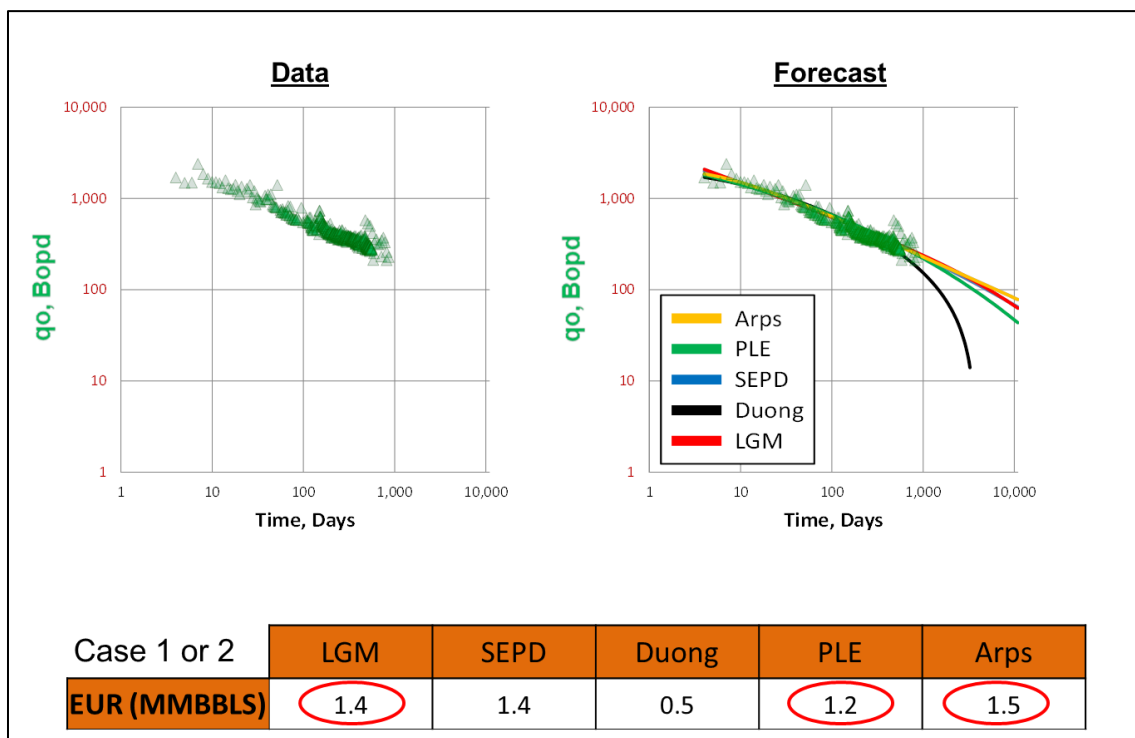


Figure 46. Linear flow for Bakken shale oil well BK-86. This well is similar to Case 1 or 2. For Case 1, Arps, LGM and PLE methods provide comparable forecasts assuming linear flow regime until abandonment. For Case 2 the forecast has to be re-run when BDF is reached.

6.3 Eagleford Shale Gas - Well EF-3

This well is an oil well from the Eagleford shale. The well shows a decline that is most similar to Case 3. If the well reaches the boundary then it becomes similar to case 4. Assuming Case 3, the best methods are the SEPD, Duong, and PLE. If Case 4 is assumed, the forecast should be re-run when boundary is reached.

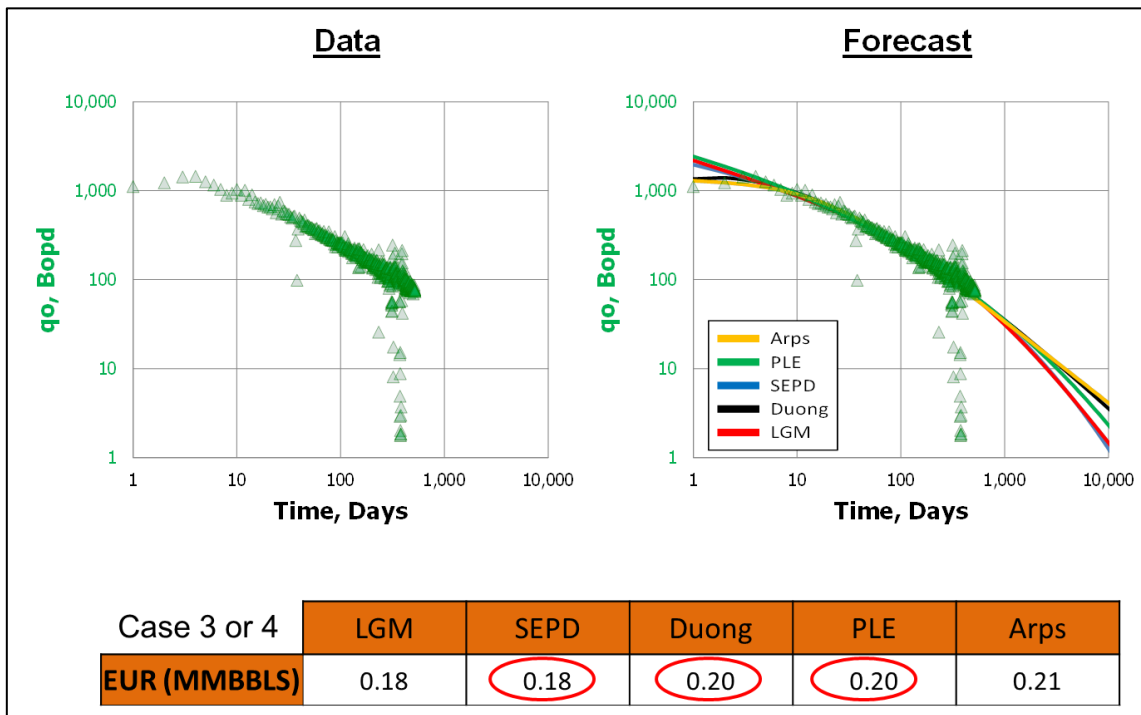


Figure 47. Eagleford well 204. This well is similar to case 3 or 4. For Case 3 the true forecast should be bracketed between Arps and the LGM method. For Case 4 the forecast has to be re-run when BDF is reached.

6.4 Fayetteville Shale Gas - Well FF-3

This well is a gas well from the Fayetteville shale. The production decline is different from all the cases that were run. Therefore it is not possible to determine which method is best. A range of possible forecast can be established from the different methods. The range is from 1.7 to 3 Bscf.

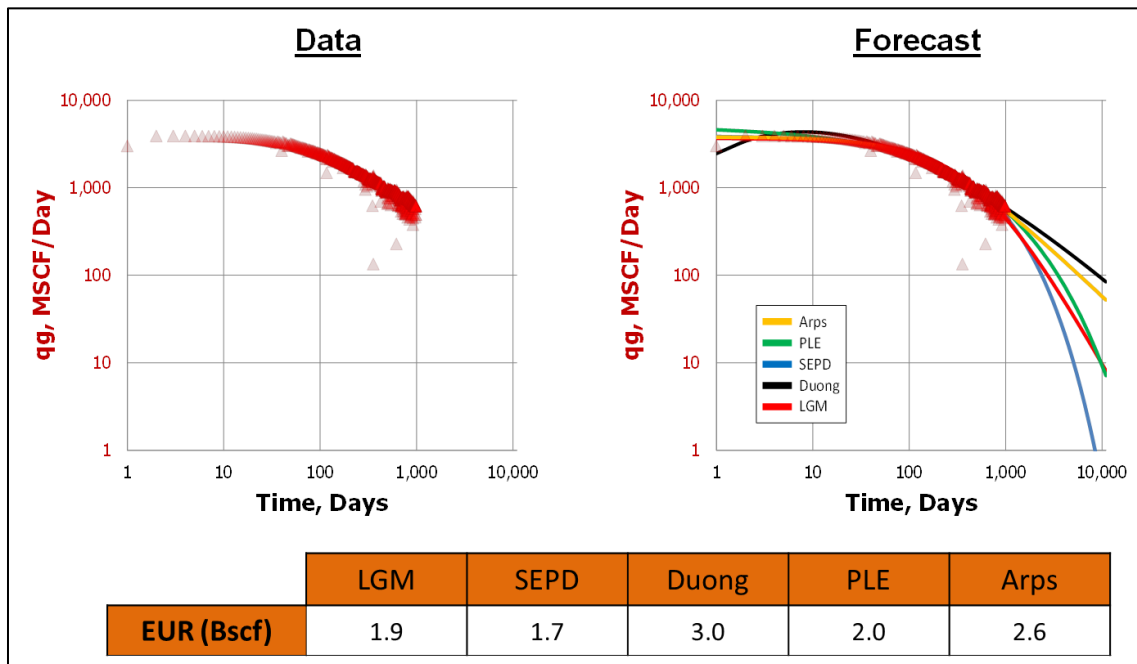


Figure 48. Fayetteville Well FF-3. The well is not similar to any of the run cases. The best method cannot be determined.

CHAPTER VII

DISCUSSION AND CONCLUSIONS

The decline methods shown here have different models and equation forms, thus often provide different forecasts. Arp's hyperbolic equation can be shaped into a straight line to fit either bilinear or linear flow with b values of 2 and 4 respectively. However, it cannot model multiple flow regimes. The PLE is the only method that models transient and BDF decline. The SEPD model is difficult to shape into a straight-line because of its equation formulation. Duong's is the only method that models clean-up while the LGM is the easiest method to use. If BDF is expected, the EUR cannot be accurately established until BDF is observed. Four cases that represent the typical flow regimes of shale wells were simulated to evaluate which method(s) is/are best for each case:

- Linear: if a well is expected to show linear flow to abandonment, the most accurate EUR is determined using Arps, PLE, or LGM. The Duong method can also be used if q_{∞} is constrained to 0.
- Bilinear-Linear: if a well is expected to show linear flow to abandonment but was preceded by bilinear flow, the most accurate EUR is determined by the PLE, SEPD, or Duong methods.
- Linear-BDF or Bilinear-Linear-BDF: if the well is expected to show BDF prior to abandonment, a reliable forecast cannot be established. The BDF must be observed to reliably estimate ultimate recovery. The method that best models both transient and BDF of shale wells is the PLE method.

In addition, the methods equation forms are investigated and improvements were suggested.

- Arps cannot fit multiple flow regimes and therefore a composite Arps' method with two different b values is suggested.
- The iteration of the PLE method might blow-up because the q_i parameter can be too large for Excel to handle. A constraint to prevent this is introduced.
- The SEPD method takes a very long time for iteration. The use of LMA reduces the time greatly.
- Duong's method cannot rigorously model linear or bilinear flow. Programmers who develop a decline program might encounter an error while validating Duong's method against linear or bilinear flow models. A correction for this error is introduced.

REFERENCES

- Ahmadi, H.A.A., Almarzooq, A.M., and Wattenbarger, R.A. 2010. Application of Linear Flow Analysis to Shale Gas Wells - Field Cases. Paper presented at the SPE Unconventional Gas Conference, Pittsburgh, Pennsylvania, USA. Society of Petroleum Engineers SPE-130370-MS. DOI: 10.2118/130370-ms.
- Arnold, R., Anderson, R. 1908. Preliminary Report on Coalinga Oil District. U.S. Geol. Survey Bull. 357 (1908) 79.
- Arps, J.J. 1945. *Analysis of Decline Curves* Original edition. ISBN 0096-4778.
- Bello, R.O. and Wattenbarger, R.A. 2008. Rate Transient Analysis in Naturally Fractured Shale Gas Reservoirs. Paper presented at the CIPC/SPE Gas Technology Symposium 2008 Joint Conference, Calgary, Alberta, Canada. Society of Petroleum Engineers SPE-114591-MS. DOI: 10.2118/114591-ms.
- Bello, R.O. and Wattenbarger, R.A. 2010. Modelling and Analysis of Shale Gas Production with a Skin Effect. *Journal of Canadian Petroleum Technology* **49** (12): pp. 37-48. DOI: 10.2118/143229-pa
- Clark, A.J., Lake, L.W., and Patzek, T.W. 2011. Production Forecasting with Logistic Growth Models. Paper presented at the SPE Annual Technical Conference and Exhibition, Denver, Colorado, USA. Society of Petroleum Engineers SPE-144790-MS. DOI: 10.2118/144790-ms.
- Duong, A.N. 2011. Rate-Decline Analysis for Fracture-Dominated Shale Reservoirs. *SPE Reservoir Evaluation & Engineering* **14** (3): pp. 377-387. DOI: 10.2118/137748-pa
- Fetkovich, M.J. 1980. Decline Curve Analysis Using Type Curves. *Journal of Petroleum Technology* **32** (6): 1065-1077. DOI: 10.2118/4629-pa
- Hubbert, M.K. 1956. Nuclear Energy and the Fossil Fuel. American Petroleum Institute API-56-007.
- Ilk, D., Rushing, J.A., Perego, A.D. et al. 2008. Exponential Vs. Hyperbolic Decline in Tight Gas Sands — Understanding the Origin and Implications for Reserve Estimates Using Arps' Decline Curves. Paper presented at the SPE Annual Technical Conference and Exhibition, Denver, Colorado, USA. Society of Petroleum Engineers SPE-116731-MS. DOI: 10.2118/116731-ms.

- Johnson, R.H. and Bollens, A.L. 1927. *The Loss Ratio Method of Extrapolating Oil Well Decline Curves* Original edition. ISBN 0096-4778.
- Lee, W.J. and Sidle, R. 2010. Gas-Reserves Estimation in Resource Plays. *SPE Economics & Management* **2** (2): pp. 86-91. DOI: 10.2118/130102-pa
- Pirson S.J. 1935. Production Decline Curve of Oil Well My Be Extrapolated by Loss-Ratio. *Oil and Gas Jnl.* (Nov. 14, 1935).
- Samandarli, O., Ahmadi, H.A.A., and Wattenbarger, R.A. 2011. A Semi-Analytic Method for History Matching Fractured Shale Gas Reservoirs. Paper presented at the SPE Western North American Region Meeting, Anchorage, Alaska, USA. Society of Petroleum Engineers SPE-144583-MS. DOI: 10.2118/144583-ms.
- Tivayanonda, V., Apiwathanasorn, S., Economides, C. et al. 2012. Alternative Interpretations of Shale Gas/Oil Rate Behavior Using a Triple Porosity Model. Paper presented at the SPE Annual Technical Conference and Exhibition, San Antonio, Texas, USA. Society of Petroleum Engineers SPE-159703-MS. DOI: 10.2118/159703-ms.
- Turner, R.G., Hubbard, M.G., and Dukler, A.E. 1969. *Analysis and Prediction of Minimum Flow Rate for the Continuous Removal of Liquids from Gas Wells* Original edition. ISBN.
- Valko, P.P. 2009. Assigning Value to Stimulation in the Barnett Shale: A Simultaneous Analysis of 7000 Plus Production Histories and Well Completion Records. Paper presented at the SPE Hydraulic Fracturing Technology Conference, The Woodlands, Texas. Society of Petroleum Engineers SPE-119369-MS. DOI: 10.2118/119369-ms.
- Valko, P.P. and Lee, W.J. 2010. A Better Way to Forecast Production from Unconventional Gas Wells. Paper presented at the SPE Annual Technical Conference and Exhibition, Florence, Italy. Society of Petroleum Engineers SPE-134231-MS. DOI: 10.2118/134231-ms.
- Warpinski, N.R. and Branagan, P.T. 1989. Altered-Stress Fracturing. *Journal of Petroleum Technology* **41** (9): 990-997. DOI: 10.2118/17533-pa
- Ye, P., Chu, L., Harmawan, I. et al. 2013. Beyond Linear Analysis in an Unconventional Oil Reservoir. Paper presented at the SPE Unconventional Resources Conference, The Woodlands, TX, USA. Society of Petroleum Engineers SPE-164543-MS. DOI: 10.2118/164543-ms.

APPENDIX A
PLE DERIVATION

This appendix shows the PLE rate-time relation derivation.

If the loss-ratio is assumed to act as a power law function, the equation is,

$$D = D_1 t^{-(1-n)} \dots\dots\dots (A - 1)$$

Where $(1 - n)$ is the slope.

This loss-ratio decrease as time increase and therefore we can add a constant D_∞ which dominates the equation at late times. This constant makes the late time behavior similar to Arps' exponential equation with $(b = 0)$.

$$D = D_1 t^{-(1-n)} + D_\infty \dots\dots\dots (A - 2)$$

Substituting this formulation of loss-ratio into the definition of the loss-ratio gives the PLE rate-time relation,

Loss-ratio

$$D = \frac{d \ln q}{dt} = \frac{1}{q} \frac{dq}{dt} \dots\dots\dots (A - 3)$$

Substituting the PLE loss-ratio into (A - 3),

$$D_1 t^{-(1-n)} + D_\infty = \frac{1}{q} \frac{dq}{dt} \dots\dots\dots (A - 4)$$

Integrating from 0 to t ,

$$\int_0^t [D_\infty + D_1 t^{-(1-n)}] dt = \int_0^t \frac{1}{q} dq \dots\dots\dots (A - 5)$$

$$D_\infty + \frac{D_1}{n} t^n = \ln(q) - \ln(q_i) \dots\dots\dots (A - 6)$$

Rearranging into final form,

$$q = q_i \exp\left(-D_\infty t - \frac{D_1}{n} t^n\right) \dots\dots\dots (A - 7)$$

APPENDIX B

DOUNG'S METHOD DERIVATION

This appendix shows Duong's method derivation.

Time and material-balance time in linear or bilinear flow are related by the following equation,

$$t = a t_{MB} \dots\dots\dots (B - 1)$$

It can be rearranged to the following,

$$q/G_p = at^{-1} \dots\dots\dots (B - 2)$$

Duong added a fiddle factor m to make the equation more general,

$$q/G_p = at^{-m} \dots\dots\dots (B - 3)$$

Rearranging,

$$\frac{q}{at^{-m}} = G_p \dots\dots\dots (B - 4)$$

Differentiating with respect to time,

$$\frac{\frac{dq}{dt} at^{-m} - q(-m at^{-m-1})}{(at^{-m})^2} = q \dots\dots\dots (B - 5)$$

Rearranging,

$$\frac{dq}{dt} = \frac{q(at^{-m})^2 - q m at^{-m-1}}{at^{-m}} \dots\dots\dots (B - 6)$$

Expanding,

$$\frac{dq}{dt} = q at^{-m} - q \frac{m at^{-m-1}}{at^{-m}} \dots\dots\dots (B - 7)$$

Rearranging,

$$\frac{dq}{q} = \left[at^{-m} - \frac{m at^{-m-1}}{at^{-m}} \right] dt \dots\dots\dots (B - 8)$$

Integrating from 1 to t ,

$$\int_{q_1}^q \frac{dq}{q} = \int_1^t \left[at^{-m} - \frac{m}{t} \right] dt \dots\dots\dots (B - 9)$$

$$\ln q \Big|_{q_1}^q = \frac{at^{1-m}}{1-m} \Big|_1^t - m \ln t \Big|_1^t \dots\dots\dots (B - 10)$$

$$\ln \frac{q}{q_1} = \frac{at^{1-m}}{1-m} - \frac{a}{1-m} - m \ln t \dots\dots\dots (B - 11)$$

Final form,

$$q = q_1 t^{-m} \exp \left\{ \frac{a}{1-m} (t^{1-m} - 1) \right\} \dots\dots\dots (B - 12)$$

APPENDIX C

TIME AND MATERIAL-BALANCE TIME RELATION

This section shows the relationship between time and material balance time for linear.

For linear flows the rate equation is the following,

$$q_D = \frac{2}{\pi} \frac{1}{\sqrt{\pi t_{Dxe}}} \dots\dots\dots (C - 1)$$

Integrating from 0 to t_{Dxe} gives the dimensionless cumulative equation,

$$Q_D = \int_0^{t_{Dxe}} q_D dt'_{Dxe} = \int_0^{t_{Dxe}} \frac{2}{\pi} \frac{1}{\sqrt{\pi t'_{Dxe}}} dt'_{Dxe} \dots\dots\dots (C - 2)$$

$$Q_D = \frac{2}{\pi} \frac{1}{\sqrt{\pi}} 2\sqrt{t'_{Dxe}} \Big|_0^{t_{Dxe}} \dots\dots\dots (C - 3)$$

$$Q_D = \frac{2}{\pi} \frac{1}{\sqrt{\pi}} 2\sqrt{t_{Dxe}} \dots\dots\dots (C - 4)$$

Dimensionless material-balance time is defined as,

$$t_{DMB} = \frac{Q_D}{q_D} \dots\dots\dots (C - 5)$$

Substituting into the material-balance time equation gives,

$$t_{DMB} = 2t_{Dxe} \dots\dots\dots (C - 6)$$

APPENDIX D

LEVENBERG-MARQUARDT ALGORITHM (LMA)

This appendix shows the Levenberg-Marquardt Algorithm.

The objective function is the sum of squares,

$$S(b + \delta) = \sum_{i=1}^n [y_i - f(x_i, b + \delta)]^2 \quad \dots \dots \dots (D - 1)$$

Where b represents the parameters as a vector and δ is the adjustment in parameters

Expanding using the Taylor series throughout the linear term,

$$S(b + \delta) \cong \sum_{i=1}^n [y_i - f(x_i, b) - J_i \delta]^2 \quad \dots \dots \dots (D - 2)$$

In vector notation,

$$S(b + \delta) \cong \|y - f(b) - J\delta\|^2 \quad \dots \dots \dots (D - 3)$$

Re-writing as,

$$(J^T J)\delta \cong J^T [y - f(b)] \quad \dots \dots \dots (D - 4)$$

This is a gradient approach and Levenberg improved the function by adding a damping factor λ .

The Levenberg-Marquardt Algorithm (LMA),

$$(J^T J + I\lambda)\delta \cong J^T[y - f(b)] \dots\dots\dots (D - 5)$$

Where I is the identity matrix.

Each iteration step, the damping factor is adjusted. If improvement in the sum of least-squares is slow, the damping factor is increased. This brings the solution faster towards the gradient descent direction. On the other hand if the increased damping parameter results in a worse sum of least-squares, the damping value from the previous step is used.